

**SHEDDING NEW LIGHT ON INTRACELLULAR SIGNALING PATHWAYS -
ESTABLISHING LIVE-CELL FLUORESCENCE IMAGING TECHNIQUES USING
GENETICALLY ENCODED FLUORESCENT BIOSENSORS**

by

HAMZA YUSUF ALTUN

Submitted to the Graduate School of Engineering and Natural Sciences
in partial fulfillment of
the requirements for the degree of Master of Science

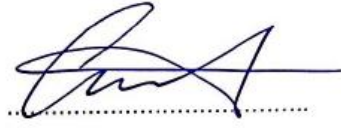
Sabanci University

August 2020

**SHEDDING NEW LIGHT ON INTRACELLULAR SIGNALING PATHWAYS -
ESTABLISHING LIVE-CELL FLUORESCENCE IMAGING TECHNIQUES USING
GENETICALLY ENCODED FLUORESCENT BIOSENSORS**

Approved by:

Dr. Emrah Erođlu
(Thesis Supervisor)



Assoc. Prof. Dr. Ali Osmay Gre



Prof. Dr. Batu Erman



Approval Date: 07/08/2020

HAMZA YUSUF ALTUN 2020 ©

All Rights Reserved

ABSTRACT

SHEDDING NEW LIGHT ON INTRACELLULAR SIGNALING PATHWAYS - ESTABLISHING LIVE-CELL FLUORESCENCE IMAGING TECHNIQUES USING GENETICALLY ENCODED FLUORESCENT BIOSENSORS

HAMZA YUSUF ALTUN

Molecular Biology, Genetics, and Bioengineering, Master's Thesis

August 2020

Thesis Supervisor: Dr. Emrah Eroğlu

Keywords: Genetically Encoded Fluorescent Biosensors, Fluorescence Microscopy, FRET, Nitric Oxide, Hydrogen Peroxide, Calcium, Acetyl-CoA

Genetically encoded biosensors are indispensable tools in cell biology and biotechnology. However, utilizing these powerful tools often require sophisticated and expensive optical imaging devices. New generations of genetically encoded biosensors are engineered as single FP based intensimetric probes that permit imaging on a single excitation and emission wavelength. In this study, we tested whether commonly used single FP based biosensors can be utilized on a simple widefield fluorescence microscope. For this purpose, we exploited a conventional and affordable epifluorescence microscope equipped with only three standard filter-sets and a three-color LED light source. We tested three differently colored biosensors including GECCO's for Ca²⁺ imaging, geNOps for NO imaging, and HyPer7 for H₂O₂ imaging. Our results demonstrate that even a low-resolution and simple microscope yields the same results as a sophisticated imaging device in terms of spatial and temporal resolution. In the second aim in these studies, we established more complex FRET imaging approaches for quantification of intracellular Ca²⁺ signals using FRET-based genetically encoded biosensors such as D3-cpV. Besides, we applied and established FRET analysis techniques with biosensors - termed as Youvan's algorithm - to increase the spatial resolution of FRET occurrence. In parallel to the FRET studies, we *in silico* designed and generated a novel FRET-based Acetyl-CoA sensor based on a bi-molecular construct differentially targeted to the cytosol and mitochondria. Overall, in these studies, we demonstrate strategies and establish (i) live-cell fluorescence imaging on a simple conventional microscope (ii) the application of FRET localization algorithms using genetically encoded FRET biosensors (iii) and design and develop FRET-based genetically encoded Acetyl-CoA sensors.

ÖZET

GENETİK KODLANMIŞ FLORESAN BİYOSENSÖRLER YARDIMIYLA FLORESAN GÖRÜNTÜLEME TEKNİKLERİ KULLANILARAK TEK HÜCRE ANALİZ YAKLAŞIMLARI

HAMZA YUSUF ALTUN

Moleküler Biyoloji, Genetik ve Biyomühendislik, Yüksek Lisans Tezi

Ağustos 2020

Tez Danışmanı: Dr. Emrah Eroğlu

Anahtar Kelimeler: Genetik Kodlanmış Floresan Biyosensörler, Floresan Mikroskopisi, FRET, Nitrik Oksit, Hidrojen Peroksit, Kalsiyum, Asetil-CoA

Genetik olarak kodlanmış biyosensörler, hücre biyolojisi ve biyoteknolojide vazgeçilmez araçlardır. Bununla birlikte, bu güçlü araçlar genellikle karmaşık ve pahalı optik görüntüleme cihazları gerektirir. Genetik olarak kodlanmış biyosensörlerin yeni nesilleri, tek bir dalga boyunda görüntülemeye izin veren tek FP tabanlı intensiyometrik problemler olarak tasarlanmıştır. Bu çalışmada, yaygın olarak kullanılan tek FP tabanlı biyosensörlerin basit bir ışık mikroskopunda kullanılıp kullanılmayacağını test ettik. Bu amaçla, yalnızca üç standart filtre seti ve üç renkli bir LED ışık kaynağı ile donatılmış geleneksel ve uygun fiyatlı bir epifloresan mikroskobu kullandık. Ca^{2+} görüntüleme için GECO'lar, NO görüntüleme için geNops ve H_2O_2 görüntüleme için HyPer7 dahil olmak üzere üç farklı renkli biyosensörü test ettik. Sonuçlarımız, düşük çözünürlüklü ve basit bir mikroskobun bile uzamsal ve zamansal çözünürlük açısından sofistike bir görüntüleme cihazı ile aynı sonuçları verdiğini göstermektedir. Bu çalışmalarda ikinci amaç da, D3-cpV gibi FRET tabanlı genetik olarak kodlanmış biyosensörleri kullanarak hücre içi Ca^{2+} sinyallerinin ölçümü için daha karmaşık FRET görüntüleme yaklaşımları oluşturduk. Ayrıca, FRET oluşumunun uzamsal çözünürlüğünü artırmak için Youvan algoritması olarak adlandırılan biyosensörlerle FRET analiz tekniklerini uyguladık ve oluşturduk. FRET çalışmalarına paralel olarak, *in silico* olarak sitozol ve mitokondriye farklı şekilde hedeflenmiş iki-moleküler bir yapıya dayanan yeni bir FRET tabanlı Asetil-CoA sensörü tasarladık ve ürettik. Genel olarak, bu çalışmalarda stratejilerimiz: (i) basit bir geleneksel mikroskopta canlı hücre floresan görüntüleme oluşturulması (ii) genetik olarak kodlanmış FRET biyosensörleri kullanarak FRET yerleştirme algoritmalarının uygulamasını (iii) ve FRET tabanlı genetik olarak kodlanmış Asetil-CoA sensörlerinin tasarlanıp geliştirilmesi.

ACKNOWLEDGEMENTS

First of all, I would like to express my deepest appreciation to my thesis advisor Dr. Emrah Erođlu for his great patience, full support, and great wisdom. He was very supportive during my studies and I would like to thank him for trusting me during my master's education. I am also thankful to Prof. Dr. Batu Erman for his endless support during my master's education. I learned a lot from his lectures. I also thank Prof. Dr. Ali Osmay Gre who taught me the baby steps of doing science. I learned how to be a patient and how to think skeptically from him.

I would like to thank my lab mates Melike Seilmiř, Yusuf Ceyhun Erdođan, Serap Sezen, Břra Nur Ata, Glřah Sevimli, and Zeynep okluk. I also thank my former lab members Dođukan Kaygusuz, Ege Can nal, and Enver Ersen for their endless friendship and support during my master's education. Also, I would like to acknowledge the great assistance of Dr. Nesibe Peker and Dr. Yunus Akko for their scientific friendship.

I would like to thank my friends Yavuz Erođlu and Can Dayıođlu for their endless support and brotherhood since the first class of Bilkent. Also, I would like to thank Simay Ayhan, Ege Dedeođlu, Ceren İncedal, Alper Poyraz, řkr Atakan, and Ahmet Kurt for their friendship and support. I also thank my friend Miray Kezer for her great support when I feel dejected. Many thanks to my high school friends Ekrem Gemci and Enes Kırveli for making me laugh when I am down.

Lastly, I would like to thank my sister Gl Altun for her great support and standing next to me during my whole life.

Above all, my deepest gratitude goes of course to my parents for just being my parents.

To The Scientific Community

TABLE OF CONTENTS

TABLE OF CONTENTS	VIII
LIST OF TABLES.....	XI
LIST OF FIGURES.....	XII
1 Introduction	1
1.1 Light and Fluorescence Microscopy	1
1.1.1 Introduction to Fluorescence Microscopy.....	1
1.2 Fluorescent Proteins	6
1.2.1 Fluorescent Proteins.....	6
1.2.2 Structure of Fluorescent Proteins	7
1.2.3 Fields of Applications of Fluorescent Proteins	8
1.3 Genetically encoded fluorescent protein-based biosensors.....	11
1.3.1 Designing Genetically Encoded Fluorescent Biosensors	12
1.3.2 Classes of Genetically Encoded Fluorescent Biosensors	14
2 Aims of the study.....	19
3 Materials	20
3.1 Chemicals and Growth Media	20
3.2 Equipment.....	21
3.3 Kits and Enzymes	22
4 Methods	24
4.1 Bacterial Cell Culture	24
4.1.1 Transformation of Genetically encoded fluorescent biosensors to Competent Bacteria.....	24

4.1.2	Plasmid Isolation	25
4.2	Plasmid Generation and Cloning strategies.....	25
4.2.1	Sequence synthesis and Codon usage optimization.....	25
4.3	Mammalian Cell Culture	26
4.3.1	Cell Culture.....	26
4.3.2	Cell Freezing	27
4.3.3	Cell Thawing.....	27
4.3.4	Transient Transfection of Cells	27
4.4	Buffer Preparations	28
4.4.1	Storage Buffer Preparation	28
4.4.2	Physiological Buffer Preparation.....	29
4.4.3	Iron(II) booster solution for NO imaging	29
4.5	Live-Cell Fluorescence Imaging	30
4.5.1	Instrumentations.....	30
4.5.2	Image Acquisition and Analysis	31
4.5.3	Statistical Analysis.....	33
5	RESULTS	34
5.1	Establishing live-cell and real-time imaging techniques on a simple and conventional LED-based epifluorescence microscope	34
5.1.1	Live-cell imaging of exogenous NO signals using the single FP-based genetically encoded NO biosensors (geNOps).....	34
5.1.2	Live-cell imaging of endogenous NO signals derived from eNOS using G-geNOps	37
5.1.3	Live-cell imaging of intracellular H ₂ O ₂ signals using the novel single FP-based and intensimetric HyPer7.1.....	41
5.1.4	Imaging mitochondrial Ca ²⁺ signals using genetically encoded GECOs	43
5.1.5	Live cell imaging of cytosolic and mitochondrial Ca ²⁺ using differentially targeted GECOs.....	44
5.1.6	Live-cell imaging of intracellular Ca ²⁺ using FRET-based genetically encoded biosensor.....	46

5.2	Design and development of a novel Acetyl-CoA biosensor	49
5.2.1	A FRET-based Acetyl CoA Sensor	49
6	Discussion.....	52
7	Conclusion	56
8	Bibliography	57

LIST OF TABLES

TABLE 1.1: LOCALIZATION SIGNALS FOR THE PROTEINS.....	10
TABLE 4.1: PRIMER SEQUENCES FOR AMPLIFICATION OF THE MITOCHONDRIA TARGETING SEQUENCE COX8	26
TABLE 4.2: SPECIFICATIONS OF FILTER SETS FOR IMAGING GENETICALLY ENCODED FLUORESCENT BIOSENSORS IN SIMPLE EPIFLUORESCENCE MICROSCOPE	30

LIST OF FIGURES

FIGURE 1.1.: PHENOMENON OF STOKES SHIFT	2
FIGURE 1.2: DIAGRAM OF PARAMETERS AFFECTING IMAGE QUALITY	3
FIGURE 1.3: LINE SPECTRUM OF MERCURY ARC LAMB.....	4
FIGURE 1.4: COMPONENTS OF WFFM	5
FIGURE 1.5: ACHIEVEMENTS IN THE FIELD OF FLUORESCENCE	7
FIGURE 1.6: PROTEIN MODEL OF GFP	8
FIGURE 1.7: PROMOTER TRACKING USING FPS.....	11
FIGURE 1.8: SCHEMATIC REPRESENTATION OF G-GENOPS.....	16
FIGURE 1.9: SCHEMATIC REPRESENTATION OF FRET BASED CALCIUM GEFB	18
FIGURE 4.1: LIVE-CELL IMAGING WITH HOME-MADE PERFUSION SYSTEM	31
FIGURE 5.1 CHARACTERIZATION OF G-GENOPS ON A SIMPE LED-BASED IMAGING DEVICE	36
FIGURE 5.2: CHARACTERIZING OF TWO DIFFERENTLY COLORED GENOPS.....	37
FIGURE 5.3: CO-EXPRESSION OF ENOS AND GENOPS IN HEK293 CELLS.....	38
FIGURE 5.4: EFFECT OF MYRISTOYLATION DEFICIENCY IN ENOS AND NO PRODUCTION.	40
FIGURE 5.5: VISUALIZING EXTRACELLULARLY ADMINISTERED H ₂ O ₂ IN THE CELL NUCLEUS USING HYPER7	42
FIGURE 5.6: CHARACTERIZING TWO DIFFERENTLY COLORED GECOS	44
FIGURE 5.7: CYTOSOLIC AND MITOCHONDRIAL CALCIUM SIGNALS USING DIFFERENTIALLY TARGETED GECOS.....	45
FIGURE 5.8: LIVE-CELL FRET IMAGING USING THE D3-CPV CALCIUM BIOSENSOR.....	47
FIGURE 5.9: SPECTRAL BLEED THROUGH AND LOCALIZATION FRET OCCURRENCE ..	48
FIGURE 5.10: DESIGN OF A NOVEL FRET BASED ACETYL COA SENSOR	50
FIGURE 5.11: VISUALIZATION OF NOVEL ACETYL COA SENSOR	51

LIST OF ABBREVIATIONS

Abbreviation	Definition
α	Alpha
β	Beta
AcCoA	Acetyl Coenzyme A
ATP	Adenosine Triphosphate
BFP	Blue Fluorescent Protein
BP	Band Pass
CCD	Charge-coupled Device
COX8	Cytochrome Oxidase 8
cpV	Circularly Permuted Venus
DIC	Differential Interference Contrast
DMEM	Dulbecco's Modified Eagle's Medium
DMSO	Dimethyl Sulfoxide
DNA	Deoxyribose Nucleic Acid
EC50	Half Maximal Effective Concentration
ECFP	Enhanced Cyan Fluorescent Protein
EDTA	Ethylenediaminetetraacetic acid
EGFP	Enhanced Green Fluorescent Protein
EGTA	Ethylene Glycol-bis(β -aminoethyl ether)-N,N,N',N'-Tetraacetic Acid
EM-CCD	Electron Multiplier Charge-coupled Device
eNOS	Endothelial Nitric Oxide Synthase
EYFP	Enhanced Yellow Fluorescent Protein
FBS	Fetal Bovine Serum
FP	Fluorescent Protein
FRET	Förster Resonance Energy Transfer
GAF	cGMP-specific phosphodiesterase, adenylyl cyclase, and FhlA
GEFB	Genetically Encoded Fluorescent Biosensors
GFP	Green Fluorescent Protein
HEK293	Human Embryonic Kidney 293
HeLa	Henrietta Lacks
IP3	Inositol 3 Phosphate
LB	Luria-Bertani
LED	Light Emitting Diode
LP	Long Pass
LSCM	Laser Scanning Confocal Microscopes

mseCFP	Monomeric Super Enhanced Cyan Fluorescent Protein
Myr-	Myristoylation deficient
NA	Numerical aperture
NO	Nitric Oxide
NOC-7	3-(2-Hydroxy-1-methyl-2-nitrosohydrazino)-N-methyl-1-propanamine
PBS	Phosphate Buffered Saline
PCR	Polymerase Chain Reaction
PEI	Polyethyleneimine
PLC	Phospho Lipase C
QE	Quantum Efficiency
RFP	Red Fluorescent Protein
RGB	Red-Green-Blue
ROI	Region of Interest
SOC	Super Optimal Culture
STED	Stimulated Emission Depletion Microscope
TIRF	Total Internal Reflection Microscopes
TPFM	Two-photon Microscope
WFFM	Wide-field Fluorescence Microscopy
WT	Wild Type
YFP	Yellow Fluorescent Protein

1 Introduction

1.1 Light and Fluorescence Microscopy

1.1.1 *Introduction to Fluorescence Microscopy*

Fluorescent tools have many advantages such as high contrast, high sensitivity, high selectivity, high brightness, and combinability of different colors that permit multichromatic detection of different analytes of interest. Most importantly, many fluorescent tools permit live-cell imaging without fixing the cells. Thus, fluorescence technologies are superior over other analytical techniques and indispensable tools in life-science. However, what is fluorescence? Fluorescence is a phenomenon that has been known for several hundreds of years. The first scientific description of fluorescence dates back to Sir William Herschel in the 18th century. He observed an interesting phenomenon during his studies when extracting plant-based compounds. He realized that transparent solutions containing quinine transformed the UV light, which came from his window to blue light. The compounds in the solution must have absorbed the invisible UV light and must have emitted light in another but longer wavelength. This phenomenon is today known as the Stokes shift (Stokes, 1852). **Figure 1.1** shows the Stokes shift of a dye which is a blue-emitting compound. As it is depicted in the figure the absorption and emission peaks are typically 50-100 nm apart. This situation may vary depending on the chromophore in the molecule.

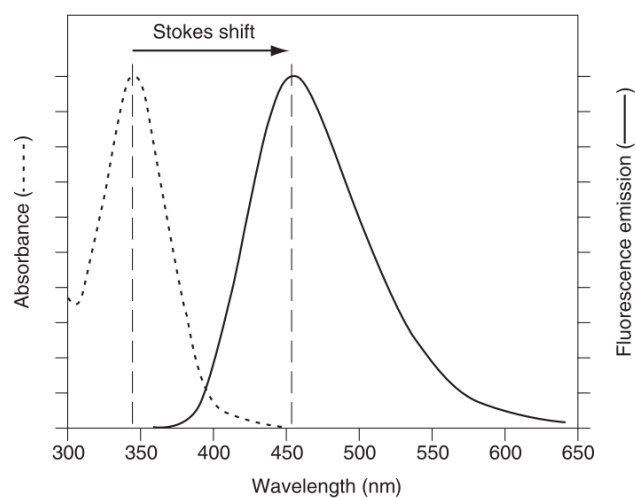


Figure 1.1.: The phenomenon of Stokes Shift: Spectrum shows the absorption and emission profiles of the dye Hoechst 33342. The dye is excited at a specific wavelength and emission is measured using spectro-fluorimeter. The difference between excitation and emission peaks is called the Stokes shift (Coling & Kachar, 1998)

After the discovery of the fluorescence phenomenon, the utilization of fluorescent probes significantly increased during the time. Many fluorescent probes were established over the past few decades. Besides fluorescent dyes of chemical nature, some naturally occurring macromolecules also have fluorescent properties, which have been exploited to investigate the structures of living cells. However, there are some considerations about fluorescence microscopy in living cells or end-point assays. One of the major challenges in fluorescence microscopy is resolution and manufacturers are trying to solve this problem via changing optical systems in a microscope (Hell, 2003). To overcome the problems in fluorescence microscopy, some terms need to be clear. In addition to the principles of microscopy, phenomena such as fluorescence, the properties of light, but also technical problems such as proper wavelength selection, recording techniques for imaging, and image analysis (Starr, 2011). The diagram in **Figure 1.2** represents how the best image can be acquired according to Combs et al (Combs, 2010). Obviously, many parameters need to be taken into consideration in high-resolution imaging.

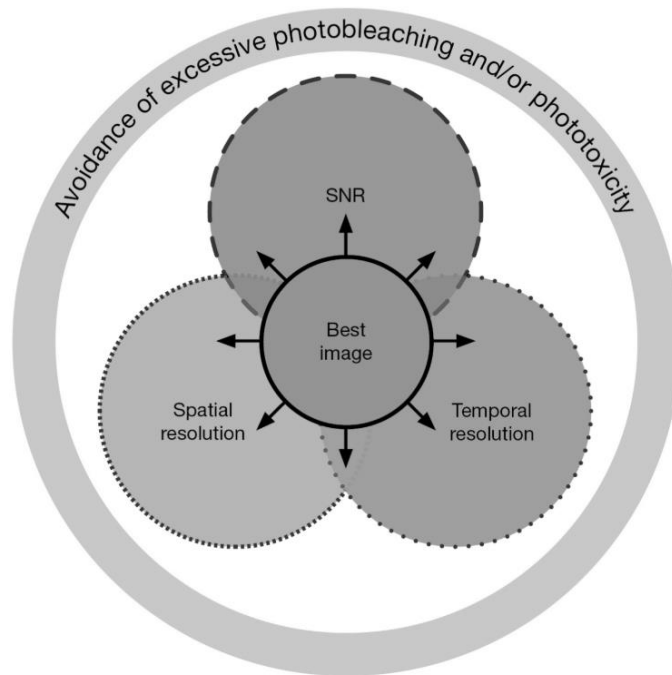


Figure 1.2: Diagram of parameters affecting image quality: According to Combs et al., how the best image can be obtained with high spatio-temporal resolution and acceptable signal to noise ratio (SNR).

1.1.1.1. *Wide-field Fluorescence Microscopy*

The most basic fluorescence microscopy technique is wide-field fluorescence microscopy (WFFM). Setup of the wide-field fluorescence microscope is consisting of the light source, filter cube, which includes excitation and emission filter and dichroic mirror, objective, and nosepiece, or camera. The working principle of wide-field microscopy can be described as follow; light is emitted via a light source and passes through the excitation filter which filters the light accordingly to the excitation wavelength of the fluorophore. A dichroic mirror reflects the monochromatic light through the objective of the sample. The red-shifted emission light from the sample passes through the dichroic mirror and subsequently positioned emission filter. The emitted light is projected to the nosepiece or the camera which is often a charge-coupled device (CCD) type (Coling & Kachar, 1998; Combs, 2010; Renz, 2013; Starr, 2011). As a light source, WFFM can have different types of light sources like tungsten-halogen, mercury-Arc lamp, metal halide, and light-emitting diodes (LED). The most recent light source is LED and has many advantages compared to other light sources in terms of precise wavelengths, power of the lamb, longer lifetime, etc. Halogen lamps are not often used in fluorescence

microscopes anymore. The main problem in halogen lamps is the incapability to sufficiently excite blue fluorophores due to the lack of UV (Masedunskas et al., 2013; Webb et al., 2004). Mercury lamps are expensive, and the main problem is the brightness of these light sources is not uniform (Davidson W. Michael, 2003). LED light sources contain narrow wavelengths of light because they have several different light sources nearly 500 times more lifetime compared to mercury lamps (Moser et al., 2006).

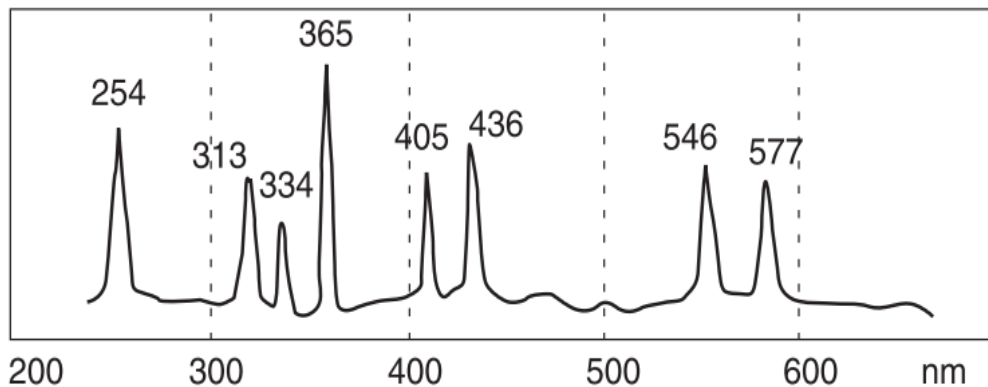


Figure 1.3: Line spectrum of a mercury arc lamp: Peaks of wavelengths are not uniform in the visible spectrum (Coling & Kachar, 1998).

The objective choice is important in fluorescence microscopy. Choosing the right objective is one of the key points in the concept of fluorescence imaging. Phase contrast objectives are not suitable for the fluorescence microscope because it blocks the incident light. Magnification and numerical aperture (NA) of the objective affect the intensity of incident light also (Masedunskas et al., 2013). The formula below shows the relation of magnification and NA between brightness (Keller, 2006).

$$\text{Brightness} \approx (NA)^4 / \text{Magnification}^2$$

After the light source, there is a filter cube that arranges the wavelength of the incident light in WFFM. The filter cube is made out of 3 colored glass mirrors: excitation filter, dichroic mirror (Angled with 45°), and emission filter. Filters are prepared by soft coating or hard coating. Soft coating means covering the glasses with vaporized low-optical index materials, but they are not durable and show a short lifetime but retain excellent reflecting properties. The hard coating of the glasses is done by metal-oxides over the surface of glasses. Hard-coated mirrors are optimal filters for fluorescence imaging because they have 100% transmission efficiency and long-lasting optical

index(Masedunskas et al., 2013). Also, the choice of the filter cube is important, especially in multispectral imaging. Each fluorophore should have one filter cube for the experiments. If there is a motorized filter turret for filter sets multicolor cubes can be used. However, they are not as effective as single-color cubes.

In WFFM CCD cameras are mainly used. The camera is consisting of an array of pixels and reflected light is captured in these arrays. RGB cameras are not useful in the fluorescence imaging because they have low resolution compared to monochromatic cameras. The quantum efficiency (QE) of the camera chip indicates how many photons reach the array of the chip. Common monochromatic CCD cameras have QE values around 60-70 meaning that 60-70% of the photons are captured by the array chip. There are also EM-CCD cameras that have a QE value of more than 90 in the visible light spectrum(Spring, 2007). In **Figure 1.4** the components of a WFFM are shown.

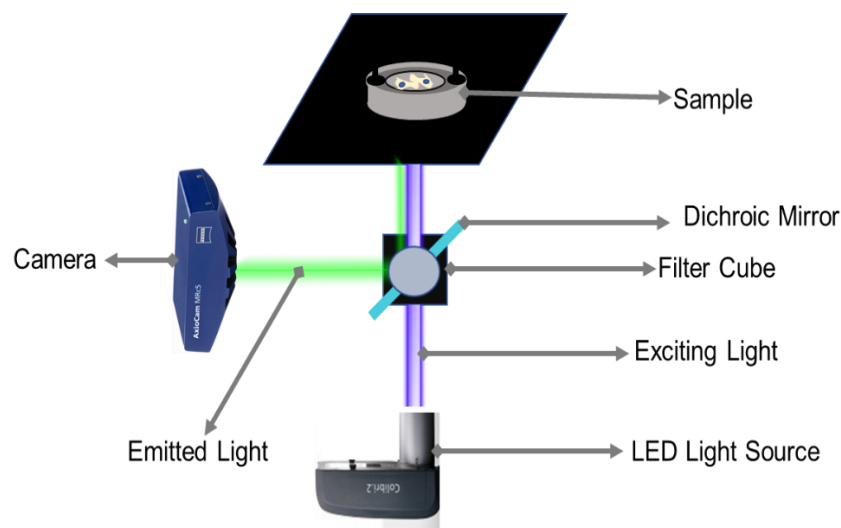


Figure 1.4: Components of WFFM: Using an LED-based light source, the excitation light passes through the filter cube and reaches the sample through the objectives. The excited sample emits light and passes through the filter cube which is reflected into the camera by a dichroic mirror.

One advantage of wide-field fluorescence microscopy is its cost-effectiveness. Wide-field fluorescence microscopy may yield high resolution in the X-Y direction of the image, but it lacks resolution in the Z direction. For deep tissue imaging, WFFM is not the best way to visualize fluorescence. Different purposes led to developing different microscope types such as laser scanning confocal microscopes (LSCM), two-photon microscopes (TPFM), stimulated emission depletion (STED) microscopes, and total internal reflection microscopes (TIRF)(Combs, 2010; Hell, 2003; Renz, 2013)

1.2 Fluorescent Proteins

1.2.1 Fluorescent Proteins

The first fluorescent proteins were discovered in jellyfish (*Aequorea victoria*) and at that time, it was termed aequorin. The inventors later named this glowing protein as the green fluorescent protein (GFP) (Shimoura et al., 1962). Due to the lack of molecular biological techniques, not earlier than 1992, the GFP was first utilized for scientific experiments (Prasher et al., 1992). Martin Chalfie conducted the first *in vivo* experiments with GFP in *C. Elegans* in 1994 (Chalfe et al., 1994). For their contribution, the three scientists Martin Chalfie, Osamu Shimomura, and Roger Tsien won the Nobel prize in Chemistry in 2008. The first cloning and application of the GFP led to an enormous interest in the studies related to FPs. Roger Tsien recognized very early the power of this technology and engineered a colorful palette of novel FP derivatives such as cyan, blue, yellow (Cubitt et al., 1995; Heim & Tsien, 1996). Soon differently colored FPs were isolated from other species such as the sea anemone *Entacmaea quadricolor* to expand the color palette of FP with orange, red, and far-red variants (Rodriguez et al., 2017). Although many species are expressing FPs naturally, for biotechnological purposes, the brightness of these FPs was insufficient, which naturally led scientists to generate synthetically improved FP versions. Using protein engineering technologies such as rationale mutagenesis or random mutagenesis new variants of chromophore structures were invented with improved brightness, pH stability, faster maturation, monomeric behavior, and narrow spectrum. Nowadays, high-throughput technologies for directed protein evolution have been established such as error-prone PCR that permits screening of millions of bacterial colonies. Undoubtedly, this field is one of the fastest-growing areas in life-sciences. In 2019, 26.695 articles were published either directly dealing with or related to GFP technologies, and this area is exponentially growing. As shown in **Figure 1.5** the timeline represents important milestones and developments in the field of FP technology (Numbers are obtained by simply searching for “green fluorescent protein” in PubMed).

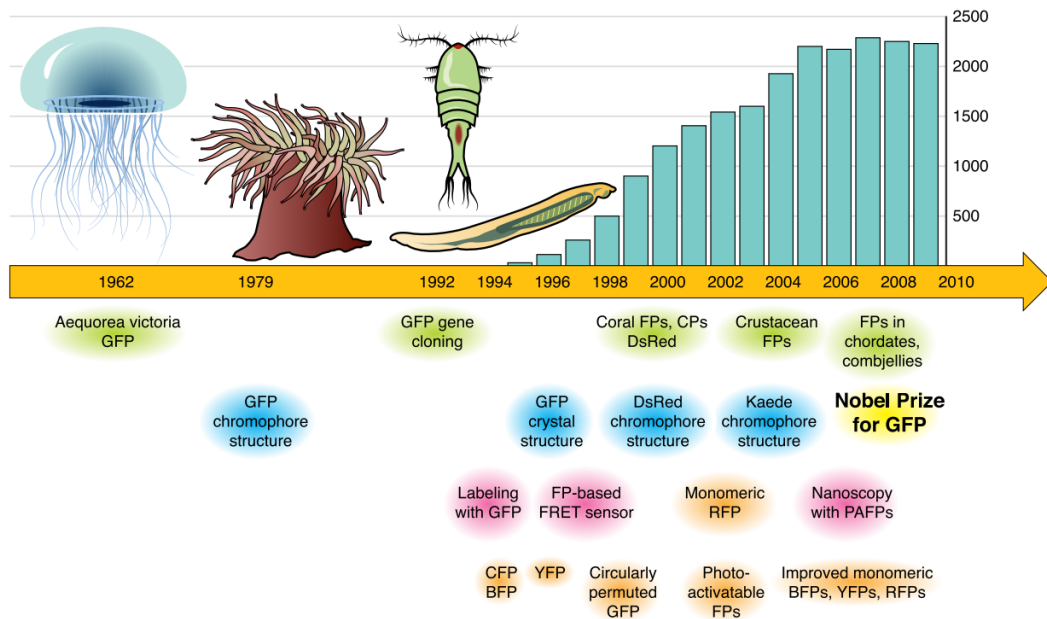


Figure 1.5: Achievements in the field of fluorescence: Animals shown in the upper part of the timeline are jellyfish, sea anemone copepod, and lancelet. Bars represent the number of published articles in the field of GFP. Below the timeline green color represents basic studies in the natural diversity of the GFP, blue color shows milestones in the structural part of the FPs, orange color indicates new FP variants derived from GFP and other FPs derived from natural FPs and purple color represents the developments in the application of FPs (Chudakov et al., 2010)

1.2.2 Structure of Fluorescent Proteins

GFP derived fluorescent proteins contain 220 to 240 amino acids and the secondary structure of the proteins are composed of 11 β -sheets and one internal distorted α helix located in the center, also distorted helix carries the chromophore of the GFP meaning that the glowing part of the protein is found in the center of barrel-shaped protein (Mats et al., 1996). The chromophore is the part of the protein that emits light and is composed of 3 well-conserved amino acid residues at position 65 to 67. Even if the residue in the 65th position may vary, tyrosine and glycine at position 66 and 67 respectively, are conserved in many of the natural FPs (Mats et al., 1996; Tsien, 1998). Beta sheets around the barrel protect the chromophore from external solvents like a shield around the chromophore, also amino acids in the barrel stabilize the protein against deterioration and provide physio-chemical resistance (Bokman & Ward, 1981; Tsien, 1998). Moreover, side chains of the amino acids in the beta-sheets, which are faced with the chromophore, have played an important role in the formation of the chromophore. Besides those amino

acid residues, which are close to the chromophore, affect catalytic events such as cyclization (Lemay et al., 2008). Mutagenesis studies unveiled the importance of residues in the beta-sheets which are near the chromophore. These are the residues 148,165,167 and 203, which can affect protonation of the tyrosine residue at position 66. Moreover, these residues affect conformation changes, polarization. Also, some beta-sheets (7, 8, and 10) can affect the spectral properties of the fluorescent protein such as red shifting of the FP (Andresen et al., 2005; Brejc et al., 1997a; Chudakov et al., 2003; Yang, 1996).

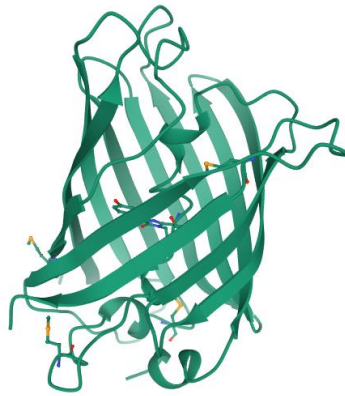


Figure 1.6: Protein model of GFP: Model is obtained from RCSB with a PDB ID:1EMA

1.2.3 *Fields of Applications of Fluorescent Proteins*

In 25 years following the cloning of the GFP, this development increased the use of FPs in various fields of biology. Fields of applications of FPs can be classified as two main groups such as structural studies and functional studies. Structural studies include labeling of the biomolecules like protein, nucleic acids, organelles, cells, and organisms. The meaning of functional studies is inclusive of promoter activity, drug screening, ROS production, sensors, protein interactions(Chudakov et al., 2010).

1.2.3.1 *Labeling of the Proteins via FPs*

Genes of interest can be produced with an FP-tag by just simply cloning them one after another and the construct can be expressed in the cells. Labeling of the proteins using FPs is the most popular technique that FPs are being used. Using these technique scientists get deeper insights about protein interaction, translocation, degradation of the proteins in real-time. Natural FPs mostly do not interfere with the tagged proteins and some custom-made FPs also work fine with the protein of interest (Shaner et al., 2007). Which termini of the protein FP should be inserted is a different question. There are studies to improve FP tag using flexible linkers, which consist of glycine-rich sequence, to prevent steric hindrance. Also, the function of the protein determines which terminus is suitable for the FP tag (Baehler et al., 2002; Moradpour et al., 2004). Another important point in protein labeling is to achieve relatively the same expression rate in multicolor imaging. Over-expression of the protein blocks the biological activities in the cell, to some extent overexpressed construct may even cause a deletion in certain domains of the interested protein (Sakaue-Sawano et al., 2008).

1.2.3.2 Subcellular Localization Studies Using FPs

The cell trafficking of the proteins proceeds according to signal peptide sequences in the protein. FPs or FP-based sensors can be targeted to different locales in the cell to study various intracellular events such as fission or fusion of organelles, promoter activity in the cell, measurements of ligands. To localize an FP to certain compartments of the cell there are consensus signaling peptides. Commonly used signal peptides that can target the FPs to the specific cell compartments are presented in **Table 1.1**. Also, tandem repeats of the signal peptides provide robust targeting of the proteins.

Table 1.1: Localization signals for the proteins: Amino acid sequences of the signaling peptides and their source (Chudakov et al., 2010)

Localization	Signal Peptide	Termini to be fused	Source	Reference
Nucleus	PKKKRKVEDA	C-terminus	SV40	(Gallegos et al., 2006)
Cytosol	LALKLAGLDI	C-Terminus	NES	(Wen et al., 1995)
ER-Lumen	MLLSVPLLLGLLGLAAAD KDEL	N-Terminus C-Terminus	Calreticulin	(Palmer et al., 2004)
Mitochondrial Matrix	MSVLTPLLLRGLTGSARRLPVPRAKIHSLGDP	N-Terminus	COX8	(Palmer et al., 2006)
Mitochondrial Membrane	MVGRNSAIAAGVCGALFIGYCIYFDRKRRSDPN MAIQLRSLFPLALPGMLALLGWWWFFSRKK	N-Terminus N-Terminus	Tom20	(Gallegos et al., 2006)
Golgi Lumen	81 amino acids of the human 1,4-galactosyltransferase	N-Terminus	1,4-Galactosyltransferase	(Gleeson et al., 1994)
Golgi Membrane	MGNLKSVAQEPGPPCGLGLGLGCGKQGPA	N-Terminus	eNOS	(Gallegos et al., 2006)
Plasma Membrane	MGCIKSKRKDNLNDDGVDMKT	N-Terminus	Lyn Kinase	(Gallegos et al., 2006)
Peroxisomal Matrix	SKL	C-Terminus		(Gould et al., 1989)

1.2.3.3 Tracking of Promoters Activity Using FPs

The translation of the FPs can be controlled by changing the promoter elements in the construct. Using this method, the activity of the promoters can be tracked. The most popular and well-known promoter activity assay is the luciferase assay. FPs can be used instead of luciferin, but they have lower sensitivity compared to luciferase assay. However, different FPs can be expressed under different promoter elements in a single vector and this enables visualization of the activity of the promoter instead of adding enzymes. One of the key considerations of the promoter tracking system is synchronizing the promoter activity versus the maturation of the FPs. One example of this problem is that even if the promoter activity stops FPs can stay stable for days and this may lead to false inferences. The solution for that problem would be the addition of a destabilization signal to FPs (Corish & Tyler-Smith, 1999). In **Figure 1.7** example of multiple promoter tracking using multiple FPs is shown.

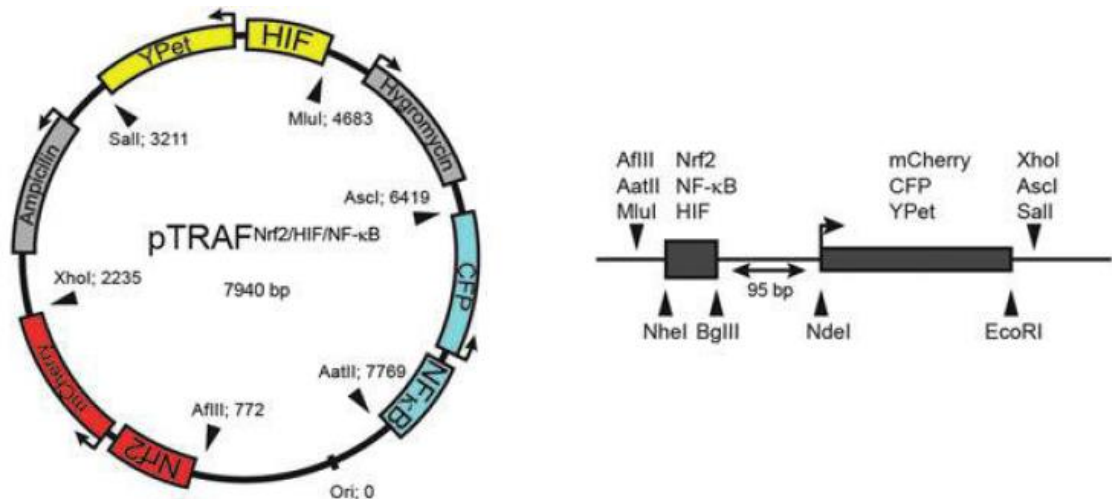


Figure 1.7: Promoter Tracking Using FPs: Johansson et al. established a vector called pTRAF which consists promoter elements of HIF, Nrf2, and NFκB and as a tracker YPet, mCherry and CFP are used respectively (Johansson et al., 2017).

1.3 Genetically encoded fluorescent protein-based biosensors

Genetically encoded fluorescent sensors have a diverse field of use. The FP itself can be genetically encoded and can be localized to different compartments in the cell. Utilizing this property of FPs, many studies exploit FPs as highlighters such as targeting mitochondria to study mitochondrial fission or fusion. FPs can be used for tracking protein-protein interaction and promoter activity (Chudakov et al., 2010; Johansson et al., 2017). Using a single laser for excitation 6 different colored FPs can be visualized under a confocal microscope which proves the power of FPs to highlight certain locales in the cell (Kogure et al., 2006). Also signaling events can be tracked without interference as in the tracking of G-coupled protein receptor activation and dissociation of IP₃ and PLC (Greenwald et al., 2018). *The use of FPs under these conditions is referred to as a passive application.*

Genetically encoded fluorescent biosensors (GEFB) are defined as chimeric proteins that can monitor signal transduction events. The main point of the engineering GEFB to monitor signaling events is that a sensor should translate a physical condition to a measurable read-out. In other words, signaling activities, conformational changes, binding of an analyte should create a signal in terms of fluorescence intensity change.

1.3.1 *Designing Genetically Encoded Fluorescent Biosensors*

As a protein chimera, GEFB consists of two domains, the first one is the sensing domain and the second one is the fluorescent protein itself. The sensing domain, as its name suggests, is responsible for detecting changes in the cellular environment and the FP domain is the reporter that conveys those changes in terms of fluorescence intensity (Frommer et al., 2009). Sequences of two protein domains are combined in a single vector and then can be expressed in interested cells. FP domain of the GEFB does not always contain a single FP, there can also be two FPs according to the application of GEFB. Interaction of the sensing and FP domains affects the signals which will be obtained. The most critical issue during the design of GEFB is to know which read-out will be obtained after the interaction. These read-outs are provided by specific analyte binding, covalent modification of sensing domain or the FP, membrane potential changes, or redox reactions (Griesbeck, 2004; Miyawaki, 2003). The first problems that scientists encounter whilst choosing the correct sensing domain are the issues related to the specificity and sensitivity of the selected domain. The sensing domain of GEFB should be specific to its ligand. For example, a protein can have two different ligands and the ligands may interact with the same binding site or a different place in the protein. In the cellular environment, two ligands may present and it affects the read-out of the GEFB. The sensing domain should be specific to its ligand, thus any competitor would disrupt the binding. Another thing to consider during the selection of an appropriate sensing domain is the interaction of the endogenously expressed selected domain and the exogenously expressed GEFB. Most of the genetically encoded calcium biosensors contain calmodulin as their sensory domains. Exogenously expressed calmodulin in the GEFB may interfere with the intracellular calcium signaling competing with endogenous calmodulin (Zarowny et al., 2020). Moreover, choosing the sensing domain from eukaryotic species is a challenging issue. Eukaryotic proteins mostly undergo post-translational modifications and they are endogenously expressed in the cell such as calmodulin. These sensing domains also interact with the intracellular protein network and this may cause artifacts (Miyawaki, 2003). A possible solution proposed for this problem is choosing a heterologous version of the interested protein as in HyPer. HyPer contains a prokaryotic H₂O₂ sensitive transcription factor as its sensing domain (Belousov et al., 2006)

Fluorescent proteins have different physical properties compared to other proteins because of their optical characteristics. Although their optical features make these proteins uniquely informative, their use in GEFB requires critical fine-tuning of optical and biochemical characteristics. Sensitivity, signal to noise ratio, maturation time of the FP, photostability, and pH stability are well-known parameters in the design of FP domains. Choosing brighter FPs is important for the sensitivity of the GEFB and it increases the signal-to-noise-ratio. As brighter FPs require minimal excitation light intensity to visualize under a microscope, phototoxicity is prevented due to minimum exposure to exciting light. FPs can be engineered by random mutagenesis to make brighter variants which can be easily selected through screening of bacterial colonies expressing random mutant FPs (Wang & Tsien, 2006; Zarowny et al., 2020). However, lower brightness is required for long-term experiments to increase photostability. The photostability of the FPs is naturally provided by its barrel shape which shields the chromophore from the cellular environment. Photostability may be a contradictive issue when performing different experiments. High photostability may decrease the sensitivity of the GEFB. Therefore, scientists engineered FPs called circular permuted FPs in which photostability of the FP is decreased (Baird et al., 1999; Luger et al., 1989). In circular permutation, the chromophore of the FPs is exposed to the cellular environment. However, the interaction of the sensing domain and FP domains is increased. Exposure to the cellular environment affects the pH stability of the FPs. Many of the FPs are pH sensitive and they have different pK_a values meaning that their brightness changes according to the pH of the environment. Under physiological conditions, pH may vary and it can cause an unreliable read-out from the GEFB. However, to overcome this problem engineered FPs which are pH stable can be used. On the other hand, this unfavorable condition can be exploited to design pH sensors (Baird et al., 1999). Turnover and maturation time of the FP domain are also important features for GEFB design. If the purpose of the experiment is to monitor dynamic cellular events such as protein interactions or promoter tracking, maturation and turnover of the FPs in the cellular environment must be as short as promoter activation or protein-protein interaction time. For that purpose, timer peptides are conjugated to FP to synchronize GEFB read-outs with promoter activation or protein-protein interaction (Subach et al., 2009).

1.3.2 *Classes of Genetically Encoded Fluorescent Biosensors*

Genetically encoded fluorescent biosensors can be classified in terms of the nature of their FPs or their read-outs such as single FP based ratiometric or intensimetric, FRET-based.

1.2.3.4 *Single FP Based GEFB*

Single FP based GEFB may contain a sensing domain or sometimes the sensing domain is the FP itself. Due to the natural structure of the FP, the chromophore is protected from the environment. However, some FPs have been engineered in a way that they can react to certain analytes/changes such as pH, metal ions, and intracellular redox state. The nature of the GFP has autocatalytic activity and the chromophore forms cyclization of amino acid residues. Chemically, the wild type GFP has two states as neutral species and anionic species. As neutral species, the amino acid residue tyrosine at Y66 is protonated and in the anionic state, it is deprotonated. The majority of the chemical state is neutral, and the two species are responsible for single emission and double excitation behavior of the GFP. Changing between these two states occurring with the proton relay between H bonds in the protein. This relay causes the chromophore to become anionic state then the proton travels through H-bonds and keeps the chromophore as its in the neutral state. The traveling of the proton and keeping chromophore in its neutral state make the GFP resistance to environmental change (Brejc et al., 1997b; Chattoraj et al., 1996). Engineered proteins such as EGFP, ECFP, EYFP have the spectrum shift compared to wild type GFP. This shift is caused by distortion in the H-bonds and it makes FP sensitive to factors such as pH (Kneen et al., 1998). Jayaramayan et al. used engineered YFP to design Cl⁻ and halide GEFB, using the H418Q mutant (Jayaraman et al., 2000). Besides, GEFB can consist of the FP only. FP domain is the messenger as it is mentioned in the previous section. The sensing domain affects the FP domain and the read-out will be the fluorescence intensity change. In terms of the read-out, two different classes of single FP based GEFB present. The first one is an intensimetric type which has an FP with a single excitation and emission peak in the spectrum. Analyte binding, protein interaction, or redox state changes affect the sensing domain of the GEFB, and the sensing domain interacts with the FP domain then the intensity of the FP changes

upon interaction. The second one is ratiometric single FP based GEFB. In this scenario, the FP domain of these GEFB consists of 2 emission maxima and one excitation maxima or vice versa. Upon the change in the sensing domain fluorescence intensity of the FP changes accordingly to its emission or excitation peaks. As an example, one FP has two excitation peaks in its spectra such as 398 nm and 478 nm and one emission peak at 510 nm. At initial state fluorescence intensity is high when excited with 398 nm (Belousov et al., 2006). Upon analyte binding fluorescence intensity obtained by exciting the FP with 398 nm wavelength decrease but fluorescence intensity obtained by exciting the FP with 478 nm increases. The ratio of the fluorescence intensities obtained by two different excitation wavelengths is the read-out of these types of GEFB (McAnaney et al., 2002). In this study, we used geNOps, Hyper, and GECOs. We used the single-FP based intensimetric variants of these GEFBs and our focus will be in this study to characterize the GEFBs. geNOps are designed for sensing NO radicals in single cells. As a sensing domain, the GAF domain of the bacterial transcription factor NorR, which can selectively bind NO has been used in this probe. GAF domain binds NO via its non-heme Iron (II) center. The sensitivity of the geNOps was determined by exposing various NO donor chemicals. Binding of NO to the GAF domain brings the NO radical in close proximity with the FP chromophore. Eroglu et al. show that proximity affects the FP domain of the GEFB because NO radical interferes with the chromophore of the FP domain. As a result, the read-out of the geNOps is an immediate loss of fluorescence (Eroglu et al., 2016). Among the palette of the geNOps we decided to use green variant g-geNOps and the schematic representation of the G-geNOP is shown in **Figure 1.8**.

The next GEFB that we characterized in this study is GECOs. GECOs are the genetically encoded calcium indicator and as a sensing domain, calmodulin and M13 were used. Read-out of the single-FP based GECOs is an increase in the fluorescence intensity. Binding of a Ca^{2+} to the sensing domain of GECO leads to a conformational change and the intensity of the FP will be increased (Kalko et al., 2011). Among the broad palette of the GECOs in this study, we used blue and red variants of the GECOs.

Hyper is the GEFB which senses intracellular H_2O_2 . As a sensing domain, Hyper contains a bacterial transcription factor called OxyR. Upon oxidization of OxyR by H_2O_2 , between C199 and C208 residues in the protein, the disulfide bond is formed. This bond formation leads to a conformational change and that change is transmitted to the fluorescent domain. Oxidization of the OxyR domain affects the spectral properties of the fluorescent domain (Bilan & Belousov, 2016). Hyper is developed since it is introduced and, in this study, we used the last version of the intensimetric nucleus targeted Hyper7.1.

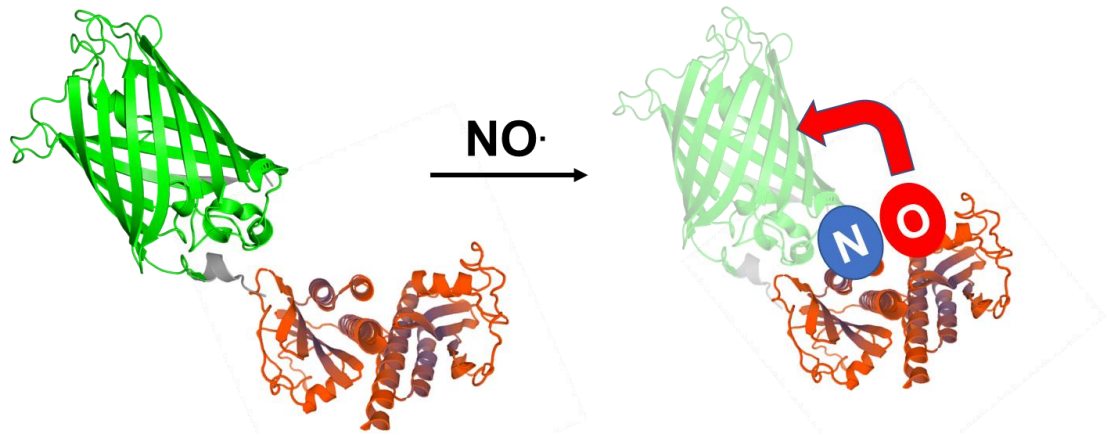


Figure 1.8: Schematic representation of G-geNOps: G-geNOp contains EGFP as a fluorescent protein and upon the presence of NO. Due to this change, NO radical and fluorescent protein get closer to each other and NO affects the chromophore of the EGFP. The red arrow shows NO-EGFP interaction.

1.2.3.5 FRET Based

FRET is the abbreviation of Förster resonance energy transfer. The so-called donor fluorophore transfers its energy to nearby so-called acceptor fluorophore in order to excite it, while only the donor fluorophore is being excited. In other words, the donor is excited, and its emission wavelength can excite the acceptor if it is in close proximity (10-100 Å) (Sekar & Periasamy, 2003) Notably, this energy transfer is nonradiative. FRET efficiency is depicted in the formula below. E stands for FRET efficiency, r is the distance between donor and acceptor and R_0 represents Förster distance (Bajar et al., 2016).

$$E = \left[1 + \left(\frac{r}{R_0} \right)^6 \right]^{-1}$$

FRET efficiency is also affected by the spectral overlap between donor emission and the acceptor excitation (Bajar et al., 2016). The most well-known FRET pair (Donor/Acceptor) is CFP/YFP but the first FRET pair that is introduced is BFP/GFP (Piston & Kremers, 2007). The reason why BFP/GFP is not a good FRET pair is caused by phototoxicity because to excite BFP it requires near UV excitation and low photostability. CFP/YFP pair provides high quantum yield, brighter FPs, with relatively closer distance when paired together comparing with other FRET pairs. However, a short distance between the pairs lowers the dynamic range, and YFP suffers from fast photobleaching (Lam et

al., 2012). New FRET pairs are mostly using the brighter GFP and RFP because of the photobleaching of the YFP.

FRET pair is mainly inserted into N and C terminus of the sensing domain to create FRET-based GEFB. Many applications of the FRET-based GEFB presents such as measuring enzymatic activity, protein-protein interaction, and also FRET-based GEFB can perfectly carry out what single FP based GEFB can do. Read-out of the FRET-based GEFB is similar to the single FP based ratiometric GEFB. If there is a FRET occurrence, excitation with 430 nm wavelength leads to emission at 535 nm but without FRET emission would be seen at 480 nm. CFP is excited at 430 nm and it emits light at 480 nm, emitted light can excite YFP within 10-100 Å distance (**Figure 1.9**). Read-out of the FRET experiments is the ratio of fluorescence intensity of 535 nm and fluorescence intensity of 480 nm emission. There are also considerations about the FRET-based GEFB like dynamic range of the FRET, amplitude of the FRET ratio, delayed or decreased on/off kinetics, photostability, pH stability. Read-out of the FRET-based GEFB is a quantitative measurement of the signal change. In the case of the longer experiments, proper folding (maturation) and folding rate can affect the read-out. For that reason, FRET pairs must be carefully considered. Faster maturation of the FPs shows great FRET performance (Scott & Hoppe, 2015). Interaction of FRET pairs under inactive condition is also important. If the pairs normally tend to interact with each other, it increases the initial FRET ratio. This is a problem for dynamic range, it prevents understanding the difference between high FRET and low FRET. To solve this problem, FPs are mutated to add more hydrophobicity to residues in order to decrease intramolecular interactions between FRET pairs (Nguyen & Daugherty, 2005). Another solution to this problem is to add linker peptides between the sensing domain and acceptor or donor FPs to decrease interaction. It shifts the distance between FRET pairs (Wriggers et al., 2005). The large size of the FPs affects the kinetics of the FRET-based GEFB. Delay of the response against stimulus is caused by a slow moment of the FPs (Piston & Kremers, 2007). Also, the dissociation of the analyte should be well considered. To increase the dissociation rate sensing domain of the GEFB should have a low affinity as it should be in the single FP based GEFB. Fast kinetics is also obtained by using circularly permuted FRET pairs (St-Pierre et al., 2014) Photostability and pH sensitivity are related to the exposure of the chromophore to the environment. To neglect the photobleaching effect, there are methods for photobleaching correction techniques. To neglect the pH effect, pH insensitive FRET pairs can be used like EYFP or Citrine instead of YFP. However, these two parameters affect the FRET ratio not intensively because

the read-out of the FRET-based GEFB is its ratio. Thus, if the two FPs are affected, the ratio of their intensities may remain the same.

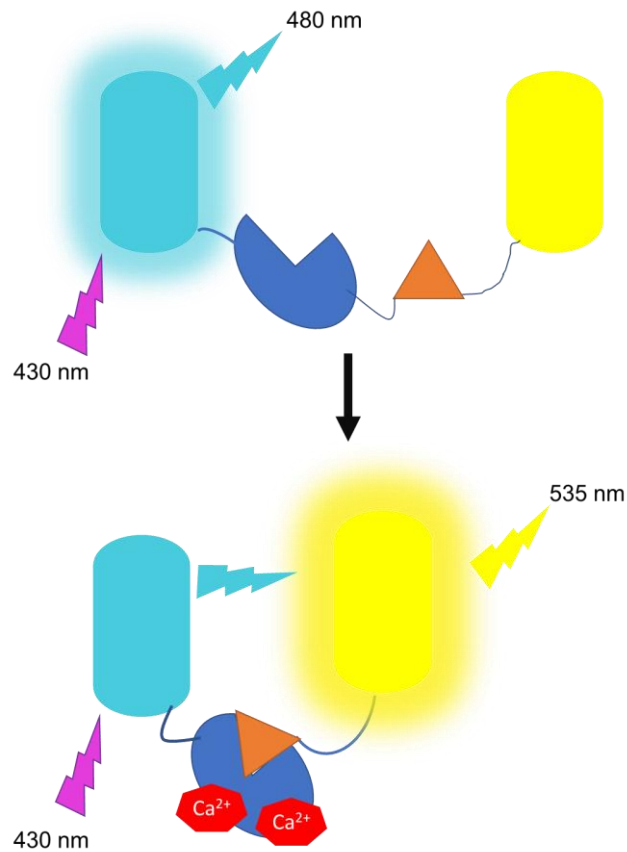


Figure 1.9: Schematic representation of FRET-based Calcium GEFB: Calcium sensing domains are paired with the FRET FPs. Under normal conditions (w/o Ca²⁺) 430 nm excitation leads to 480 nm emission. In the presence of Ca²⁺, calcium-sensing domains undergo a conformational change, and FRET pairs get closer. Then 430 nm excitation leads to 535 nm emission because of the FRET.

2 Aims of the study

Genetically encoded fluorescent biosensors are powerful tools that can be exploited to unveil cell signaling events under pathophysiological conditions. Many sophisticated devices were developed to increase the efficiency of these tools. Also, many of these devices may not be found in standard laboratories and these restrictions affect the broad applicability of genetically encoded biosensors. We aimed here to test whether conventional and affordable imaging devices that are almost present in any lab can be refitted without the need for sophisticated accessories to employ genetically encoded fluorescent biosensors. Thus, in this study, I used a simple and conventional LED-based epifluorescence microscope to characterize various genetically encoded fluorescent biosensors for Ca^{2+} , NO, and H_2O_2 . Moreover, I also aimed to design and apply an in-house made gravity-based perfusion system for the administration and withdrawal of various pharmacological drugs and buffers during the imaging experiments.

My second aim was to test and characterize FRET-based sensors on a sophisticated high-resolution device. For this purpose, I tested the Ca^{2+} sensor termed as D3-cpV. Besides simply imaging FRET signals, I also aimed to establish a FRET localization technique with genetically encoded FRET biosensors that was described after the inventor and termed as the Youvan algorithm.

In my third aim, I attempted to *in silico* design, generate and test a novel FRET-based Acetyl CoA sensor for live-cell imaging of Acetyl CoA levels in subcellular locales.

3 Materials

3.1 Chemicals and Growth Media

Chemicals and Growth Media	Company
Dulbecco's Minimal Essential Medium	PAN-Biotech, Germany
Fetal Bovine Serum	PAN-Biotech, Germany
Penicillin/Streptomycin	PAN-Biotech, Germany
Trypsin-EDTA 0.25%	PAN-Biotech, Germany
Liquid Broth	Sigma-Aldrich, USA
SOC Medium	New England Biolabs, USA
Ampicillin	Sigma-Aldrich, USA
Kanamycin	Sigma-Aldrich, USA
Glycerol	neoFroxx, Germany
Dimethyl sulphoxide	PAN-Biotech, Germany
Phosphate Buffered Saline	PAN-Biotech, Germany
Calcium Chloride	neoFroxx, Germany
Potassium Chloride	neoFroxx, Germany
Sodium Chloride	neoFroxx, Germany
Magnesium Chloride	neoFroxx, Germany

D(+) Glucose	neoFroxx, Germany
Adenosine Triphosphate	Sigma-Aldrich, USA
Histamine	Sigma-Aldrich, USA
Iron (II) Fumarate	Alfa Aesar, USA
L-Ascorbic Acid	neoFroxx, Germany
MEM Vitamins	PAN-Biotech, Germany
HEPES	PAN-Biotech, Germany
L-Glutamine	PAN-Biotech, Germany
Sodium Pyruvate	PAN-Biotech, Germany
Sodium Bicarbonate	neoFroxx, Germany
Monopotassium Phosphate	neoFroxx, Germany
PolyJet USA	SignaGen Laboratories,
Serum-Free Phenol Red Free DMEM	PAN-Biotech, Germany
Isopropanol	Merck, Germany
Sodium Hydroxide	Sigma-Aldrich, USA
EGTA	Sigma-Aldrich, USA
Hydrogen Peroxide	neoFroxx, Germany
NOC 7 USA	Santa Cruz Biotechnology,

3.2 Equipment

Equipment	Company
Fluorescence Microscope	Carl Zeiss, Germany

Light Microscope	Carl Zeiss, Germany
20X Objective	Carl Zeiss, Germany
Filter Sets	Carl Zeiss, Germany
Light Source	Carl Zeiss, Germany
Camera	Carl Zeiss, Germany
Biosafety Hood	Nüve, Turkey
CO ₂ Chamber	Nüve, Turkey
Waterbath	Nüve, Turkey
Heat Block	Eppendorf, Germany
Tabletop Centrifuge	Eppendorf, Germany
	Beckman-Coulter, USA
Hemocytometer	Isolab, Germany
Shaking Incubator	New Brunswick, USA
ThermoCycler	BioRad, USA
NanoDrop	Thermo-Scientific, USA
pH Meter	Ohaus, USA
Cell Freezing Container	Mr. Frosty, USA

3.3 Kits and Enzymes

Molecular Biology Kits	Company
Mini-prep DNA Isolation	Macherey-Nagel, Germany
Midi-prep DNA Isolation	Qiagen, Germany
Taq Polymerase PCR Kit	Thermo-Fischer, USA

Gel Purification and PCR Clean-Up

Qiagen, Germany

Enzymes

EcoRI

HindIII

KpnI

NheI-HF

NotI

Company

New England Biolabs, USA

New England Biolabs, USA

New England Biolabs, USA

New England Biolabs, USA

New England Biolabs, USA

4 Methods

4.1 Bacterial Cell Culture

4.1.1 *Transformation of Genetically encoded fluorescent biosensors to Competent Bacteria*

The bacterial transformation was achieved by following the instructions provided by the company New England Bioscience. Commercially available *E.Coli* DH5 α strains were used. 10 μ l competent bacteria were thawed on ice and 2 μ l plasmid solution corresponding to 1pg -1 μ g DNA were mixed in a 1.5 ml reaction tube. Following a 30 minutes incubation on ice, cells were heat-shocked in a heating block for 30 seconds at 42°C. Cells were then immediately transferred to an ice bucket and further incubated for 5 minutes. After this step, 900 μ l SOC (room temperature) media was added to the bacterial-plasmid mixture and incubated for 1 hour at 37° C in a conventional shaking incubator at 220 rpm. Only 200 μ l of the mixture was plated on an LB-Agar plate containing appropriate antibiotics. Plates were incubated at 37° C for 16 hours. Single colonies were picked to inoculate 3 ml of liquid LB media containing appropriate antibiotics. After further incubation for 16 hours, 100 μ l of the bacterial solution was mixed with 500 μ l sterile glycerol (50% (v/v)) and snap frozen. Tubes were than kept at -80° C for long-term storage.

4.1.2 Plasmid Isolation

50 ml of LB media containing the respective antibiotic of a concentration (100 U/ml) was transferred into a sterile Erlenmeyer flask and inoculated with 50 µl of the bacterial glycerol stock and incubated at 37° C for 16 hours in a conventional shaking incubator with a speed around 220 rpm. Plasmid DNA isolation was performed using a commercially available Qiagen MidiPrep kit according to the instructions of the manufacturer. The purity and concentration of the isolated plasmids were determined using a spectrophotometer. The isolated plasmid was kept at 4° C for further usage or stored at -80° C for long-term storage.

4.2 Plasmid Generation and Cloning strategies

4.2.1 Sequence synthesis and Codon usage optimization

For the generation of novel constructs including PanD (NCBI Reference Sequence:NC_000913.3:c146694-146314) and PanZ (NCBI Reference Sequence:NC_000913.3:3597984-3598367), the sequences were obtained using NCBI Gene search engine. For a FRET-based genetically encoded sensor the FRET pair mseCFP and cpVenus were used. For the design of a single FP-based genetically encoded sensor, cpGFP fluorescent protein sequence was obtained from Addgene. To make constructs targeted to the mitochondria, the COX8 targeting sequence was used. For codon usage optimization online tools and algorithms were used from the websites www.Jcat.de or www.twistbioscience.com to achieve proper expression in mammalian cells. Synthesized constructs were subcloned into cytomegalovirus (CMV) driven mammalian expression vectors referred to as pTwist-BetaGlobin. Subcloning was achieved by applying the Gibson Assembly method with the restriction sites NotI and NheI on the N-terminus and C-terminus, respectively. For mitochondria targeting sequence insertion, primers were designed to PCR-amplify the COX8 gene in tandem. As a template, the mito-R-GECO plasmid was used and the restriction sites NotI and EcoRI were introduced. The PCR- amplicon was inserted using restriction digestion

methods into the mammalian expression vector pTwist-BetaGlobin. Primers for mitochondria targeting sequence are shown in **Table 4.1**.

Table 4.1: Primer sequences for amplification of the mitochondria targeting sequence COX8

<i>Primer Name</i>	<i>Sequence (5'→3')</i>
<i>NotI-Mito-YFP-For</i>	<i>ATAGCGGCCGCATGTCGTCTGACTCCTCTG</i>
<i>EcoRI-Mito-YFP-Rev</i>	<i>TATGAATTCTTGAAGAGTCGACCATGGTTGG</i>
<i>NotI-Mito-CFP-For</i>	<i>ATAGCGGCCGCATGTCGTCTGACTCCTCTG</i>
<i>EcoRI-Mito-CFP-Rev</i>	<i>ATAGAATTCTCTGAAGAGTCGACCATGGTTG</i>

4.3 Mammalian Cell Culture

4.3.1 Cell Culture

HEK293, HeLa, cell lines were obtained from various sources. (ATCC, CRL-1573, ATCC, CCL-2) For maintenance, all type of cells were cultured on 10 cm or 30 cm cell culture dishes using complete Dulbecco's modified Eagle's medium (Complete DMEM), which includes serum-free DMEM, 10% (v/v) heat-inactivated FBS, 100 U/ml penicillin and 100 µg/ml streptomycin mixture. Cells were incubated in a humidified CO₂ incubator at 37 °C and 5% CO₂. When cells reached 100% confluency, the growth media was aspirated and washed with D-PBS. Splitting was achieved by incubating cells for 3 to 5 minutes in a pre-warmed Trypsin-EDTA solution. To verify that all cells were detached, a conventional phase-contrast light microscope (Carl Zeiss, Germany Primovert, 20x Objective) was used. To deactivate the enzymatic activity of trypsin complete DMEM was added to the cell suspension and further collected into a 15 ml tube. Cells were split into new cell culture dishes with a ratio of 1:5 and 1:10. After 24 hours the growth media was replaced by fresh complete DMEM.

4.3.2 *Cell Freezing*

Before cell freezing, a cell freezing medium containing complete DMEM and 10% DMSO was prepared and chilled to 4 °C. Confluent cells were collected by trypsinization as described above. Using a tabletop centrifuge, cells were pelleted at 1800 RCF for 5 minutes at 18° C. The supernatant was discarded, and the cell pellet was resuspended using an ice-cold cell freezing medium. Cells from one 10 cm cell culture dish were used for a single cryovial corresponding to 7.5 million cells. Cryovials were put in a cell freezing box which contains isopropanol ensuring a gradual freeze. Then the cryo box was stored in -80 °C for 24 hours. For short-term storage, vials were kept in -80 °C or transferred into a liquid nitrogen tank for long-term storage.

4.3.3 *Cell Thawing*

The frozen cryovials were immediately incubated in a 37 °C water bath for quick thawing (~60 seconds) until most of the cell suspension was thawed. Pre-warmed 1 ml of complete DMEM was added to the cryovial and transferred to a 15 ml tube. An additional 8 ml pre-warmed complete DMEM was added to the cell suspension and seeded onto a 10 cm cell culture dish. After a 24-hour incubation at 37 °C with 5% CO₂, the old medium was replaced with a fresh full medium.

4.3.4 *Transient Transfection of Cells*

Approximately 100,000 to 200,000 cells were seeded onto a 6-well plate containing 30mm round-shaped glass-coverslip on or two days, respectively before the transfection. When cells reached 70% confluency the old media was replaced with a fresh medium 1 hour before the transfection step. Two different transfection approaches were tested in this study:

A: Transfection using Polyethyleneimine (PEI): For one well of a 6-well plate 100 μ l serum and phenol-red-free minimal essential medium, 1 μ g of plasmid DNA and 3 volume of DNA content PEI were mixed in a 1.5 ml tube. The mixture was incubated at room temperature for 30 minutes. For one well of a six-well plate 100 μ l of the transfection mixture was dropwise added and gently moved in south-north and east-west directions following incubation in the cell culture chamber. 6 hours after the transfection procedure, old media was replaced by a prewarmed full medium. Cells were imaged after 24h or 48 hours post transfection.

B: Transfection with PolyJet[®] Two 1.5 ml tubes were prepared while the first tube contained 100 μ l antibiotic and phenol-red free high-glucose DMEM and 1 μ g of interested DNA. The second tube was prepared using 100 μ l media and 2.5 μ l PolyJet for one well of a six-well. After the addition of PolyJet, both mixtures were immediately mixed without vortexing. Following a 15 min incubation time at room temperature, the DNA-PolyJet mixture was dropwise added to the cells. Maximum 3 hours after the transfection medium was replaced and 24 or 48 hours later imaged.

4.4 Buffer Preparations

4.4.1 Storage Buffer Preparation

Briefly, a storage buffer (EH-Loading) is a media similar to a complete DMEM without FBS and phenol red. The storage buffer was used to incubate cells for 20-30 minutes before live-cell imaging experiments to allow the cells to equilibrate to the environmental conditions. The following recipe was used to prepare a storage buffer 135 mM NaCl ,. 2 mM CaCl₂ , 1 mM MgCl₂, 10 mM HEPES, 5 mM KCl , 2.6 mM Na₂HCO₂ , 0.44 mM KH₂PO₄ , 0.34 mM Na₂HPO₄, 0.1% essential amino acids , 0.2% MEM vitamins , 2 mM L-glutamine, 10 mM glucose x 1 H₂O, and 100 U/ml penicillin and 100 μ g/ml streptomycin mixture. The pH of the buffer is adjusted to 7.42 using 1 mM NaOH and all ingredients are mixed using a stirring plate. Using a 0.22 μ m medium filter, the storage buffer was sterile filtered, separated into aliquots, and stored at 4 °C for later usage.

4.4.2 *Physiological Buffer Preparation*

Live-cell imaging experiments were performed using a HEPES-based physiological buffer. Two different imaging buffers were used in the experiments according to the purpose of the study. The Ca^{2+} containing physiological buffer, referred to as 2-CaNa contained: 2 mM CaCl_2 , 1 mM MgCl_2 , 138 mM NaCl , 5 mM KCl , 10 mM glucose and 10 mM HEPES per 1000 ml H_2O . The pH of the buffer was adjusted to 7.42 using 1 mM of NaOH . All ingredients were stirred using a stirrer plate until all chemicals were dissolved. This buffer was prepared freshly before the experiments and stored at room temperature until use. If a Ca^{2+} free buffer was needed, the same recipe was used except using 2mM Ca^{2+} but instead, 1mM EGTA was added to the solution to achieve a 0 Ca^{2+} solution.

4.4.3 *Iron(II) booster solution for NO imaging*

geNOps are a class of biosensors containing a non-heme based iron center. To supply the proper amount of reduced Fe^{2+} to cells, treatment with iron(II) and vitamin C containing buffer was prepared for this purpose. Iron(II) containing buffer was prepared using 2-CaNa buffer as described in the previous section above. 1 mM of iron(II) fumarate and 1 mM of ascorbic acid was added to 50 ml of 2-CaNa. The solution was stirred using a stirrer plate at exactly 2 hours under darkness and room temperature. The following filtration using a 0.22 μm syringe filter was applied to retard the unsolved iron(II) particles from the solution. If not immediately used, the solution was kept at +4 °C for a maximum of 1 week. Fresh preparation of this solution was always preferred.

4.5 Live-Cell Fluorescence Imaging

4.5.1 Instrumentations

Live-cell imaging experiments were performed using an AxioVertA1 inverted fluorescence microscope and Axio Observer 7 inverted fluorescence microscope (Carl Zeiss, Germany AG, Germany) with equipped with a 20x Carl Zeiss, Germany Plan Apochromat (20x/0.8) objective. The light source was a LED-based system of the model Colibri 2 containing the wavelengths 365 nm for blue, 470 nm for green, 555 nm for red and 625 nm for far-red. For imaging red, green, and blue fluorescent protein-based genetically encoded fluorescent biosensors the filter sets shown in **Table 4.2** were used.

Table 4.2: Specifications of filter sets for imaging genetically encoded fluorescent biosensors on a simple epifluorescence microscope

<i>Fluorescent Protein</i>	<i>Biosensor</i>	<i>Filter Set#</i>	<i>Excitation Filter</i>	<i>Dichroic Filter</i>	<i>Emission Filter</i>
<i>TagRFP</i>	R-GECO	43	545/25 BP	570 LP	605/70 BP
<i>EGFP</i>	G-geNOp	38	470/40 BP	495 LP	525/50 BP
<i>cpGFP</i>	Hyper7.1	38	470/40 BP	495 LP	525/50 BP
<i>TagBFP</i>	B-GECO	49	365 LP	395 LP	445/50 BP
<i>mKO.x</i>	O-geNOp	43	545/25 BP	570 LP	605/70 BP
<i>CFP</i>	D3-cpV	-	Colibri 7 430 nm	FT 455 BS	480/40 BP
<i>FRET</i>	D3-cpV	-	Colibri 7 430 nm	FT 455 BS	525/50 BP

The addition and withdrawal of various buffers, agonists, and inhibitors to cells were made in-house by exploiting 3-D printing technologies (**Figure 4.1**). The perfusion system was designed with six 50 ml syringe tubes connected to the perfusion chamber via capillary tubing. The perfusion chamber consisting of an inlet and outlet was connected to a peristaltic pump (200 rpm * min⁻¹) to maintain a continuous flow of around 1 ml * min⁻¹. Schematic of the instrumentation that was used for live-cell imaging is depicted in **Figure 4.1**

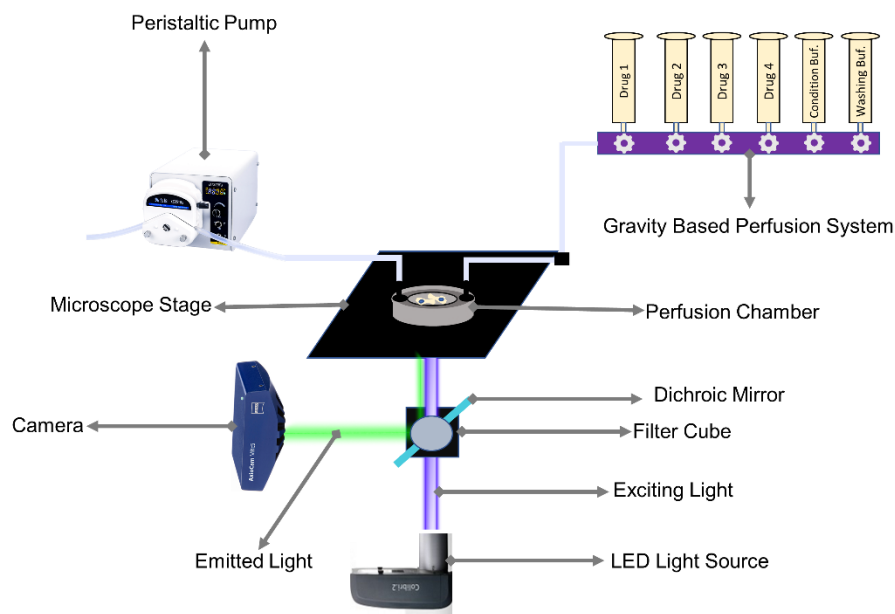


Figure 4.1: Live-cell imaging with home-made perfusion system: Schematic representation of home-made perfusion system with six independent reservoirs. The perfusion chamber is a metal-based construct permitting the safe and sealed positioning of 30 mm coverslips with living cells

4.5.2 Image Acquisition and Analysis

Live-cell imaging experiments were recorded in time-lapse (3 seconds interval) with a proper fluorescence light exposure and LED intensity for each genetically encoded biosensor using Zen Pro Software (Carl Zeiss, Germany AG, Germany). To avoid phototoxicity, all time-lapse imaging experiments were performed with binning 4x4. This allows reducing the light power and exposure with significantly reduces fluorescence bleaching. Typical light intensity was set to 3-10% for GFP, up to 20% for BFP, and 5-10% for RFP. Exposure was set between 50 and 800 milliseconds. After recording, for further image analysis region of interests (ROIs) covering single cells and in addition, a cell-free region as a background was determined. For each ROI sum of the fluorescence intensity over time was extracted to an Excel file. Background value was subtracted from the ROIs representing cells. The background-subtracted values were depicted as F_{1-n} . Fluorescence bleaching correction was performed using a one-phase decay model. To create this model, basal fluorescence intensity values were used and executed in GraphPad Prism Software version 5 (GraphPad Software, USA). Values that are

obtained from this model, represented as F_0 , were used to determine fluorescence fold change in percent using the formula below.

$$\Delta Fluorescence Intensity(\%) = \left(\left| 1 - \left(\frac{F_n}{F_0} \right) \right| \right) \times 100$$

For FRET experiments as a ratio FRET Channel, Intensity/CFP Channel Intensity is used. For localization analysis, ImageJ plug-in FRET Localizer was used. For the calculations, three types of groups of images were used. The first group of images was the cells that are expressing only donor fluorescent protein and the second group of images was the cells that are expressing only acceptor fluorescent proteins. The last group of images was the cells that expressing FRET pair meaning that they were both expressing donor fluorescent protein and acceptor fluorescent protein. All the images are obtained using donor, acceptor, and FRET channels. (Excitation/Emission, Donor Channel: 430/480, FRET Channel: 430/525, Acceptor Channel: 515/535). For the bleed-through and FRET colocalization images were executed according to guidelines (Amaral et al., 2013). Above mentioned plug-in executes Youvan correction using the formula below (DC Youvan et al., 1997)

$$F_c = F_b - \left(\frac{F_d^b}{D_d^b} \right) \times D^b - \left(\frac{F_b^a}{A_a^b} \right) \times A^b$$

Notation of the formula was explained as follows X_u^y

Substitution of X using D, A, F letters stand for the channel of the image were obtained, donor channel, acceptor channel, FRET channel respectively. The subscript and the superscript can be substituted with d, a, f and it stands total pixel intensity of the cells were expressing donor fluorescence, acceptor fluorescence, and FRET fluorescence and b stands for total pixel intensity of the background. All of the pixel intensities were calculated using monochromatic images. As an example, A_a^b stands for pixel intensity of image obtained using acceptor channel cells that are expressing acceptor fluorescence protein and the total pixel intensity of acceptor fluorescence is subtracted from the total background pixel intensity. In the above-mentioned formula, values are shown in the parenthesis stands for “pure donor pixel” and “pure acceptor pixel”.

4.5.3 Statistical Analysis

All experiments were conducted in triplicate. Statistical analysis was calculated using GraphPad Prism Software version 5 (GraphPad Software, USA). A student's t-test was applied to evaluate the significance of paired values. P values lower than $p < 0.05$ were considered as significantly different. The level of significance was determined by the *p-value*. All data are shown in \pm SD. Technical replicates are indicated as $n = x$ and the number of total cells is indicated as $/X$. For example, $n = 3/28$ means that this particular experiment was repeated 3 times and in total 28 cells were analyzed.

5 RESULTS

5.1 Establishing live-cell and real-time imaging techniques on a simple and conventional LED-based epifluorescence microscope

5.1.1 *Live-cell imaging of exogenous NO signals using the single FP-based genetically encoded NO biosensors (geNOps)*

geNOps are genetically encoded fluorescent biosensors for NO imaging, which are available in five different colors (cyan, blue-green, green, yellow, and orange). Due to the lack of a suitable microscope for high-resolution live-imaging with a set of different optical filters, in this study, we attempted to test the single GFP-based and intensimetric variant of the geNOps, termed G-geNOps. These biosensors consist of an enhanced GFP (EGFP), which is directly conjugated to a NO-sensitive domain, termed GAF (cGMP-specific phosphodiesterases, adenylyl cyclases, and FhIA), which is a subunit of a bacterial transcription factor norR (**Fig5.1 A**). Nitrosylation of the GAF domain brings the NO radical in close vicinity to the chromophore and leads probably to a local pH shift or electron transfer between the aminoacids ultimately leading to a quench of the fluorescence intensity (**Fig5.1 A**). To date, the geNOps has been only used on high-resolution microscopes equipped with light-sources other than light-emitting diodes (LED). To test the functionality of geNOps on a LED-based low-resolution microscope, we decided to use HEK293 cells because of multiple advantages such as easy transfect and the lack of an enzyme that is capable to produce NO, which are important features for the characterization of a NO sensitive biosensor. To stimulate geNOps, we used a well-known NO donor called NOC-7 (3-(2-Hydroxy-1-methyl-2-nitrosohydrazino)-N-methyl-1-propanamine). Notably, 1 mole of NOC-7 produces 2 moles of free available

NO radicals. For this purpose, we transiently transfected HEK293 cells with G-geNOps, and administrated NOC-7 using an in-house made gravity-based perfusion system. As shown in the pseudocolored images in **Figure 5.1 B**, NOC-7 reduced the fluorescence intensity, indicating the functionality of the probes. Next, we tried to test whether the duration of exposure to the NO donor affects the fluorescence intensity in HEK293 cells expressing G-geNOp. Treatment with 10 μ M NOC-7 for 30 seconds and 15 seconds, respectively, showed a clear difference in the geNOps amplitude (**Figure5.1 C**) and area under the curve (21.99 ± 3.43 for 15 seconds exposure, 64.02 ± 4.69 for 30 seconds exposure). To investigate, whether longer or shorter exposure time to NOC-7 affects the G-geNOps kinetics, we calculated the fluorescence intensity change rate over time. As shown in **figure5.1 D** the initial slope of geNOps response remained unaffected when cells were exposed to NOC-7 for 30 seconds or 15 seconds. Our data show that the sensitivity of our imaging system is sufficient to resolve even small temporal changes. Besides, our data are in line with the first article describing geNOps, where the authors demonstrated that G-geNOps amplitude reached around 18% while in our experiments we reached 15% of fluorescence change in response to the same concentration of NOC-7. Overall, we demonstrate here that a simple LED-based imaging device (Axiovert A1 equipped with Colibri 2) with a low-resolution objective yields high-quality readouts compared to high-end sophisticated imaging devices, which has been used in all the studies utilizing geNOps.

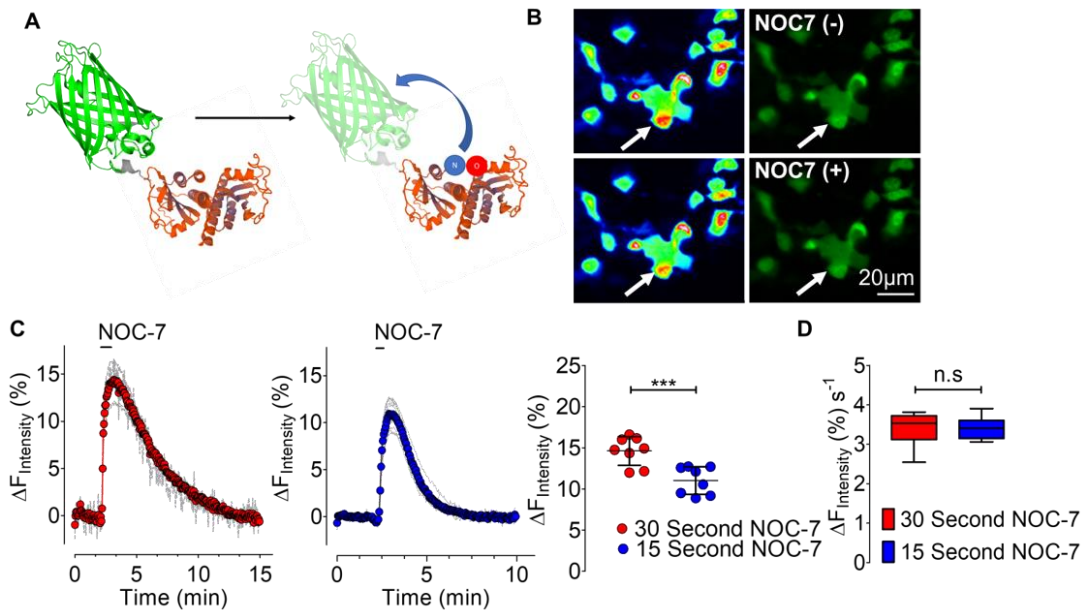


Figure 5.1 Characterization of G-geNOps on a simple LED-based imaging device: (A) Cartoon shows the principle of G-geNOps, which consists of an EGFP and the NO sensitive GAF domain. In the presence of NO, EGFP fluorescence intensity decreases. **(B)** Low resolution representative widefield images showing HEK293 cells expressing G-geNOp. Fluorescence images were obtained before (upper panels) and after stimulation (lower panels) with 10 μM NOC-7. Arrows indicate a loss of fluorescence intensity in response to NOC-7. **(C)** Average curves show G-geNOps responses to 10 μM NOC-7 in HEK293 cells expressing the probe. Cells were stimulated for 30 seconds (left panel, red curve, n=3/9) and 15 seconds (right panel, blue curve, n= 3/9) with 10 μM NOC-7. Light grey curves show individual cell responses. Maximum fluorescence intensity changes of cells, red dots for 30 seconds exposure, and blue dots for 15 seconds exposure, represented as scatter dot-plot. Data are shown as ±SD (Student's t-test was applied, *p-value* <0.001). **(D)** The whiskers box represents the fluorescence change rate of cells exposed to NOC-7 for 30 seconds (red box, n= 3/9) and 15 seconds (blue box, n=3/9). The student's t-test yielded no significant difference. Data are shown in ±SD. Cells were imaged with a 20x air objective in a low-resolution mode of camera binning 4x4 yielding.

geNOps are available in five different spectral properties. Because of the limited availability of filter sets, we attempted to test the red-shifted orange variant of geNOps using standard Red-FP filter cubes. Notably, the orange spectrum of O-geNOps-NES is relatively close to the green filter settings and no maximum emission can be collected with the red-filter cube used in the current studies **Figure 5.2C**. As shown in **Figure 5.2A** HEK293 cells were transiently transfected with G-geNOps and O-geNOps, respectively and both constructs showed robust and efficient expression profiles. Short cell treatment with the NO-donor NOC-7 instantly increased the G-geNOps signals as expected. However, unexpectedly, the O-geNOps signals showed a similar NO response (**Figure 5.2B**). Notably, this O-geNOps showed in our instrumental imaging setup almost 40%

stronger NO response compared to all previous studies in which the same experimental conditions have been used.

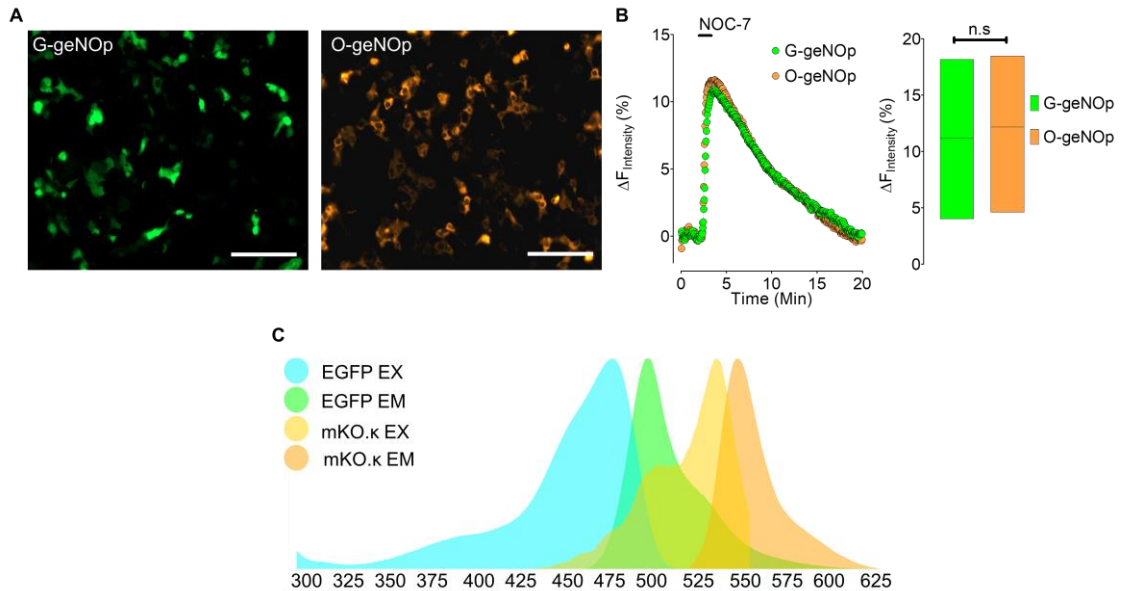


Figure 5.2: Characterizing of two differently colored geNOps : (A) Representative fluorescence images show HEK293 cells expressing G-geNOp (right panel) and O-geNOp (left panel). The scale bar represents 100 μm . (B) HEK293 cells expressing the respective geNOps were exposed to 10 μM NOC-7. The orange curve represents O-geNOps expressing cells ($n=3/28$) and the green curve represents G-geNOp expressing cells ($n=3/24$). The box plot shows the maximum responses of cells expressing G-geNOp (green box) and O-geNOp (orange box). Data are shown in $\pm\text{SD}$ (Student's t-test, $p\text{-value} > 0.05$) (C) Panel shows the excitation and emission spectra of mKO.k and EGFP as indicated.

5.1.2 Live-cell imaging of endogenous NO signals derived from eNOS using G-geNOps

In mammalian cells, NO is produced by specialized enzymes called nitric oxide synthase (NOS). In endothelial cells, the endothelial nitric oxide synthase isoform (eNOS, or NOS3) is predominantly expressed. As shown in **Figure 5.3A**, in its inactive state eNOS is bound to the cholesterol-rich part of the plasma membrane called caveolae and Golgi membrane via myristoylation. Myristoylation permits eNOS to be bound to caveolae. Based on the current literature, myristoylation deficient eNOS (further abbreviated as myr⁻ eNOS) is less active compared to WT eNOS. To test the NO production capacity of these two eNOS variants (WT- eNOS vs eNOS myr⁻), we used again HEK293 cells.

Transiently transfected HEK293 cells with myr eNOS-RFP and WT- eNOS RFP showed a clear and robust expression profile (**Figure 5.3B** upper Panel). For NO imaging, these cells were co-transfected again with the green G-geNOps. (**Figure 5.3B** middle Panel).

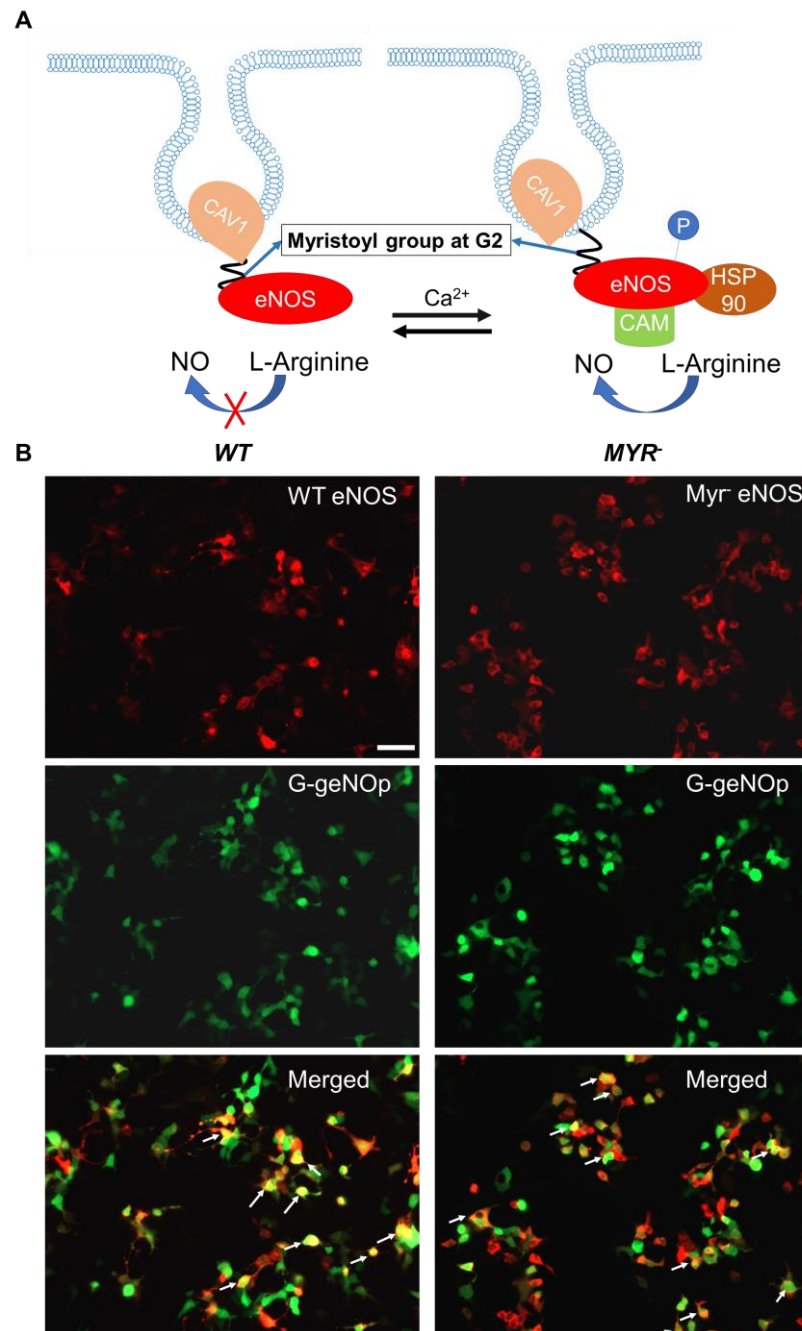


Figure 5.3: Co-expression of eNOS and geNOps in HEK293 cells : (A) Schematic shows activation of eNOS upon stimulation. Under normal conditions, eNOS is tethered to caveolae in its inactive form (left scenario). (B) Representative fluorescence images show HEK293 cells expressing WT eNOS-RFP, myr- eNOS RFP respectively, as indicated. Cells were co-transfected with g-geNOps. The lower panel shows merged representative widefield images. White arrows indicate cells that are expressing both eNOS variant and g-geNOps. The scale bar represents 50 μ m.

To activate eNOS we used various pharmacological tools such as IP3-generation agonists including histamine and ATP. As shown in **Figure 5.4A**, ATP yielded the most robust intracellular Ca^{2+} signals in HEK293 cells, imaged with the well-established red-shifted genetically encoded Ca^{2+} indicator, termed GECO (**Figure 5.4A**). Compared to histamine, ATP evoked even after re-addition a prominent intracellular Ca^{2+} elevation. Physiological concentrations of histamine did not trigger comparable Ca^{2+} signals in HEK293 cells even when administered before ATP (data not shown). We next tested whether HEK293 cells expressing the WT or myr- variant of eNOS co-expressing G-genOps show any difference in their NO formation capacity. To reduce basal NO activity triggered by extracellular Ca^{2+} or intracellular Ca^{2+} leak, cells were imaged in an extracellular Ca^{2+} free imaging media additionally containing the Ca^{2+} chelator ethylene glycol-bis(β -aminoethyl ether)-N,N,N',N'-tetraacetic acid (EGTA). Under these imaging conditions, cell treatment with extracellular ATP yielded in WT eNOS RFP expressing HEK293 cells a robust and clear NO signal as expected (**Figure 5.4B**). Removal of the GCPR ligand from the media instantly led to the geNOps signal recovery to the baseline. Subsequent exposure to NOC-7 showed a strong NO signal. These data are consistent with former studies showing NO profiles in HEK293 cells expressing the WT eNOS RFP construct. However, to our surprise, the myristoylation deficient eNOS variant, which was supposed to generate fewer amounts of NO in comparison to the WT variant showed the same NO profiles under the same experimental conditions (**Figure 5.4B**). Overall, our data demonstrate against the current knowledge in the literature that myristoylation deficient eNOS is as potent as the WT eNOS in terms of NO formation capacity.

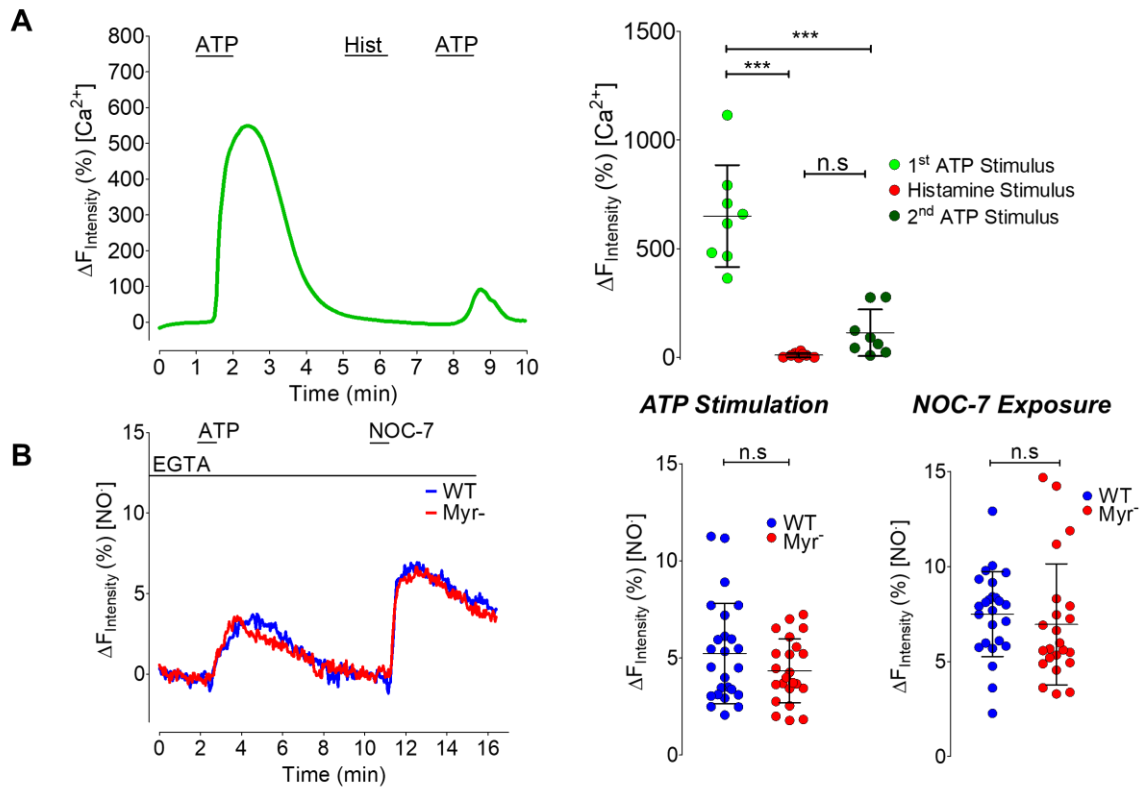


Figure 5.4: Effect of myristoylation deficiency in eNOS and NO production : (A) Mean curve shows HEK293 cells expressing R-GECO1 in response to 100 μM ATP, 5 μM histamine, and 100 μM ATP stimulation. A scatter dot plot shows maximum responses for two IP₃ generating agonists (ATP and histamine). Data are shown as $\pm\text{SD}$ ($n=3/8$, One-way ANOVA, p -value < 0.001 and p -value > 0.05) (B) Curves show HEK293 cells expressing WT-eNOS (blue curve, $n=3/24$) and myr-eNOS (red curve, $n=3/22$) in response to 100 μM ATP and 10 μM NOC-7 as indicated. Cells were imaged in Ca^{2+} -free and EGTA containing buffer. The left scatters dot plot shows geNOps responses of HEK293 cells expressing WT eNOS (blue dots, $n=3/24$) and myr- eNOS (red dots, $n=3/22$) under Ca^{2+} free conditions upon stimulation with 100 μM ATP. Data are shown as $\pm\text{SD}$ (Student's t -test, p -value > 0.05). The right scatters dot plot shows geNOps responses of cells expressing WT eNOS (blue dots, $n=3/24$) and myr- eNOS (red dots, $n=3/22$) upon exposure to 10 μM NOC-7. Data are shown as $\pm\text{SD}$ (Student's t -test, p -value > 0.05).

5.1.3 *Live-cell imaging of intracellular H₂O₂ signals using the novel single FP-based and intensimetric HyPer7.1*

Hyper7.1 is a genetically encoded sensor, which reports hydrogen peroxide (H₂O₂) concentrations on single-cell levels and subcellular locales. The biosensor is composed of two *E. Coli* derived bacterial transcription factors termed as OxyR domains, which are capable of sensing low levels of H₂O₂. Between the two OxyR domains, a circularly permuted GFP (cpGFP) is sandwiched. Upon binding of H₂O₂, the fluorescence intensity of the Hyper7.1 increases (**Figure 5.5A**). Upon oxidization of OxyR, the regulatory domain C199 residue forms a disulfide bond with the C208 residue leading to a conformational change and further an increase in fluorescence intensity of cpGFP (Bilan & Belousov, 2016). In this study, we test the first time the sensitivity of HyPer7.1 to extracellular H₂O₂. For this purpose, we transfected HEK293 cells with Hyper7.1-NLS, which is an intensimetric variant of HyPer with a nuclear localization signal. As shown in **Figure 5.5** the biosensor showed correct targeting to the cell nucleus. To test the sensitivity of HyPer7.1-NLS we exposed cells to different concentrations of H₂O₂ including 4, 8, 16, 32, 64 μ M H₂O₂. As expected, higher concentrations of extracellular H₂O₂ showed an instant increase in the HyPer signal which quickly reached the plateau phase indicating its full oxidation within a few seconds. Logarithmic reduction of the concentration showed clearly slower oxidation of the probe reflected by a slower on-kinetic. In line with the literature, the lowest concentration of extracellular H₂O₂ we could detect in living cells with an intact membrane amounted to \sim 8 μ M H₂O₂. Lower concentrations below 8 μ M did not affect the HyPer signal because of the permeability limit of the cell membrane to extracellular H₂O₂. This approach yielded an EC₅₀ of 23.5 μ M for the nuclear-targeted HyPer7.1. Notably, here we show the first time the diffusability-rate of extracellular H₂O₂ to the nucleus (**Figure 5.5B**). It has been shown that the time required to reach the maximum response of HyPer1 in the nucleus amounts to 4,24 minutes. Compared with our results, we demonstrate that the new HyPer7.1 is ultrasensitive to extracellular H₂O₂ and also confirms the quick diffusability of extracellular H₂O₂. Our approach demonstrates that 64 μ M H₂O₂ reaches the cell nucleus in HEK293 cells within 45 (\pm 15) seconds and demonstrates once again that a simple epifluorescence microscope permits reliable and robust imaging of H₂O₂ on the level of individual cells.

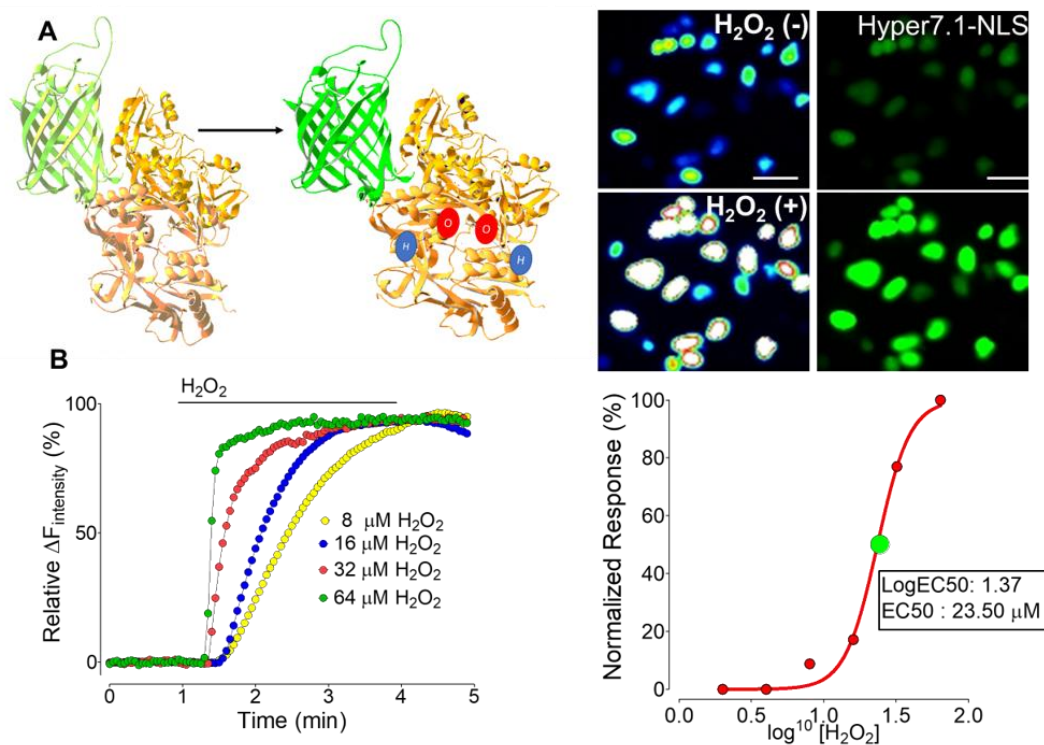


Figure 5.5: Visualizing extracellularly administered H₂O₂ in the cell nucleus using HyPer7
: (A) Cartoon represents the 3D-structure model of HyPer7.1 consisting of a cpGFP and two OxyR domains. In the presence of H₂O₂ fluorescence the GFP intensity increases. Representative microimages show HEK293 cells transfected with HyPer7.1-NLS, which contains a nuclear localization signal. Images were obtained in the presence or absence of extracellular 16 μM H₂O₂. The scale bar represents 20 μm. (B) Relative mean curves show Hyper7.1-NLS expressing HEK293 cells stimulated with various concentrations of H₂O₂ as indicated in the figure. Each experiment was performed in triplicated. The number of cells ranges from 8 to 20. The right panel shows EC₅₀ as normalized response vs log concentration of H₂O₂. EC₅₀ value yielded 23.5 μM for extracellular H₂O₂ for HyPer7.1 NLS.

5.1.4 *Imaging mitochondrial Ca²⁺ signals using genetically encoded GECOs*

In this section, we attempted to test the well-known GECO probes to image subcellular Ca²⁺ signals under different physiological conditions. GECOs consists of a circularly permuted FP sandwiched between calmodulin and M13 domains which can bind Ca²⁺ and undergoes conformational rearrangement upon interaction. GECOs are nowadays available in many different spectral properties, including ratiometric and intensimetric biosensors and different colors ranging from blue to deep red. Because of the lack of proper filter sets on our imaging device, we decided to continue our studies with the intensimetric and red and blue variant of GECOs, termed R-GECO1 and B-GECO1, respectively. After successfully implementing the green and orange biosensors as described before, we next attempted to try spectrally different GECOs. Because of the limited filter cubes on our imaging systems, we used the standard DAPI imaging filter settings to test the blue variant of GECOs termed as B-GECO. Unfortunately, we could not test other blue-shifted GECO sensors such as GEM-GECO and GEX-GECO because of their ratiometric nature, which requires double excitation at different wavelengths or collection of the emission at a different wavelength, respectively. Thus, we compared the performance of the untargeted variant of R-GECO and B-GECO in HeLa cells. As expected, HeLa cells showed robust expression of both probes (**Figure 5.8A**). To trigger intracellular Ca²⁺ release, we used histamine in the absence of extracellular Ca²⁺, which is a commonly used Ca²⁺ imaging releasing protocol to empty the ER Ca²⁺ store. As expected, the R-GECO signal instantly increased and quickly recovered in response to histamine (**Figure 5.8B**). As expected, the B-GECO showed a similar profile, however, the fluorescence change upon cell treatment was significantly lower in the amplitude but faster in the on-kinetic. Overall, our data show that standard DAPI filter sets are suitable for imaging of B-GECO. If equipped with a single multi-band pass filter set, both, the B- and R-GECO might be suitable for multispectral simultaneous imaging of Ca²⁺ signals on the level of individual cells (**Figure 5.8C**)

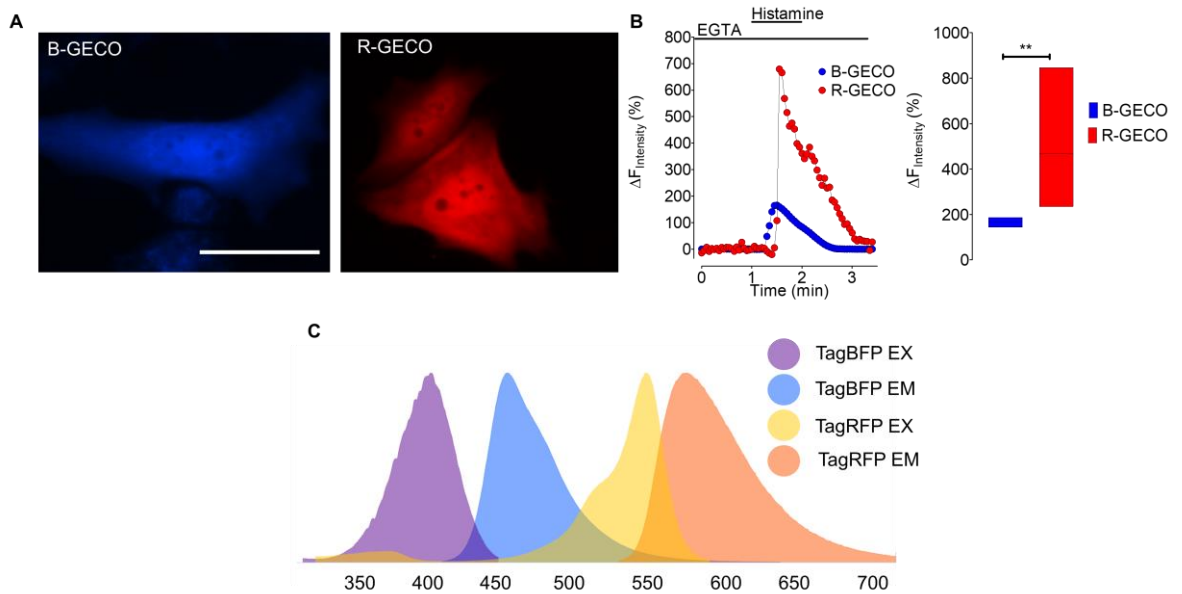


Figure 5.6: Characterizing two differently colored GECOs: (A) Representative widefield images showing HeLa cells expressing B-GECO (left panel) and R-GECO (right panel), scale bar represents 20 μm . (B) HeLa cells expressing GECOs were stimulated with 4 μM of Histamine between. Experiments were performed in the absence of extracellular Ca^{2+} and 1 mM EGTA. (n=3/6). The next box plot shows the maximum responses of cells expressing B-GECO (blue box, n=3/6) and R-GECO (red box, n=3/10). Data are shown in $\pm\text{SD}$ (n=3/6, Student's t-test, p-value < 0.01) (C) Graph shows a plot of the excitation and emission spectra of TagBFP and TagRFP, which are the FPs used in the respective biosensors.

5.1.5 Live cell imaging of cytosolic and mitochondrial Ca^{2+} using differentially targeted GECOs

GECOs can be targeted to different compartments of the cell to obtain Ca^{2+} signals in various compartments. In this section, we aimed to observe Ca^{2+} signals in the cytosol and mitochondria. For that purpose HeLa cells transiently transfected with a red variant of GECO to two different compartments of the cell. Images of positively transfected HeLa cells are shown in **Figure 5.7A**. HeLa cells expressing these biosensors were individually stimulated with ATP and fluorescence intensity changes were recorded as shown in **Figure 5.7B**. In both compartments, we observed a clear and robust Ca^{2+} elevation. Ca^{2+} elevation in the cytosol was higher compared to mitochondria. Next, we compared the maximum responses of cells expressing the GECO variants. Cytosolic Ca^{2+} elevation was significantly higher compared to mitochondria (**Figure 5.7B**). To gain more insight into the Ca^{2+} kinetics in the different compartments of the cells, we compared to Ca^{2+}

elevation rate in the cytosol and mitochondria (**Figure 5.7B**). Our results suggest that Ca^{2+} elevation rate in the mitochondria is significantly faster compared to the cytosol.

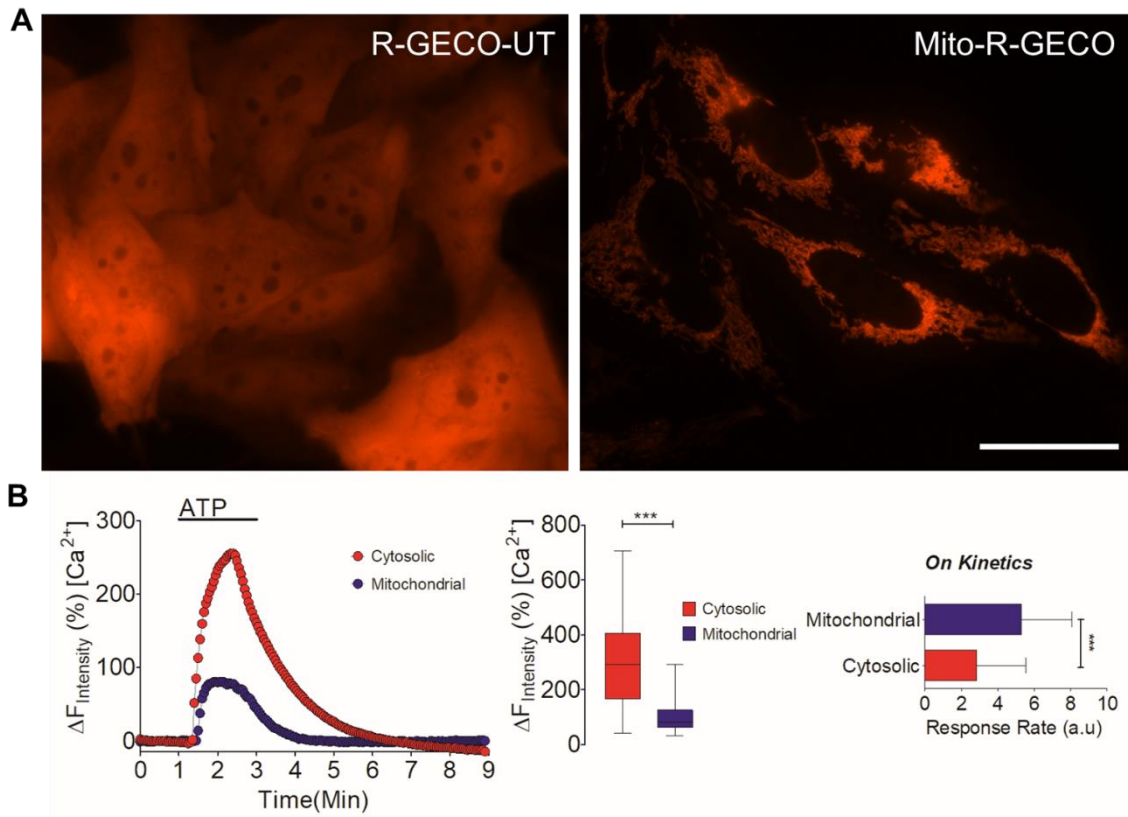


Figure 5.7: Cytosolic and Mitochondrial Calcium Signals using differentially targeted GECOs (A) Representative widefield images show HeLa cells expressing R-GECO-UT (Left panel) and Mito-R-GECO (Right panel) respectively. The scale bar represents 20 μm (B) Time course graphic shows the Ca^{2+} profiles of HeLa cells expressing R-GECO-UT (Red, Cytosolic) or Mito-R-GECO (Blue, Mitochondrial) upon stimulation with 100 μM ATP as indicated. The middle panel represents maximum responses of the cells expressing R-GECO-UT (Red box, Cytosolic, $n=3/50$) or Mito-R-GECO (Blue box, Mitochondrial $n=3/50$). Data are shown in $\pm\text{SD}$ (Student's t-test, p -value < 0.001). The graphic in the left panel shows the response rate of each sensor (R-GECO-UT, Red box, cytosolic and Mito-R-GECO, Blue box, Mitochondrial) ($n=3/50$). Data are shown in $\pm\text{SD}$ (Student's t-test, p -value < 0.001).

5.1.6 *Live-cell imaging of intracellular Ca²⁺ using FRET-based genetically encoded biosensor*

Besides the single FP based intensimetric biosensors, there are also double FP- and FRET-based genetically encoded fluorescent biosensors for Ca²⁺ imaging. Other than intensimetric biosensors, FRET-based biosensors permit quantification of its ligand in cells. In order to quantify intracellular Ca²⁺ levels under the same experimental conditions as shown in the previous sections, here we used the well-established FRET-based Ca²⁺ sensor termed as D3-cpV. We transiently transfected HEK293 cells with the D3-cpV, which showed robust expression profiles as shown in the representative images in **Figure 5.8A**. Cells were stimulated again with ATP to release intracellular Ca²⁺ from the ER store. As expected, the fluorescence intensity of the CFP (FRET donor) decreased and the fluorescence intensity of circularly permuted Venus (cpV) (FRET acceptor) increased. Removal of ATP from the imaging media quickly led to the recovery of the signals to its initial baseline. In a post-experimental analysis, the acceptor channel signals were divided by the donor channel signals, which yielded a ratiometric signal. As shown in **Figure 5.8C**, the initial baseline in a cell population ranges between 2.5 and 3.5 indicating a heterogeneity between individual cells. Notably, these experiments were obtained on an advanced epifluorescence microscope with a range of filter sets and automatic switch between different filters to enable us to collect the FRET emission.

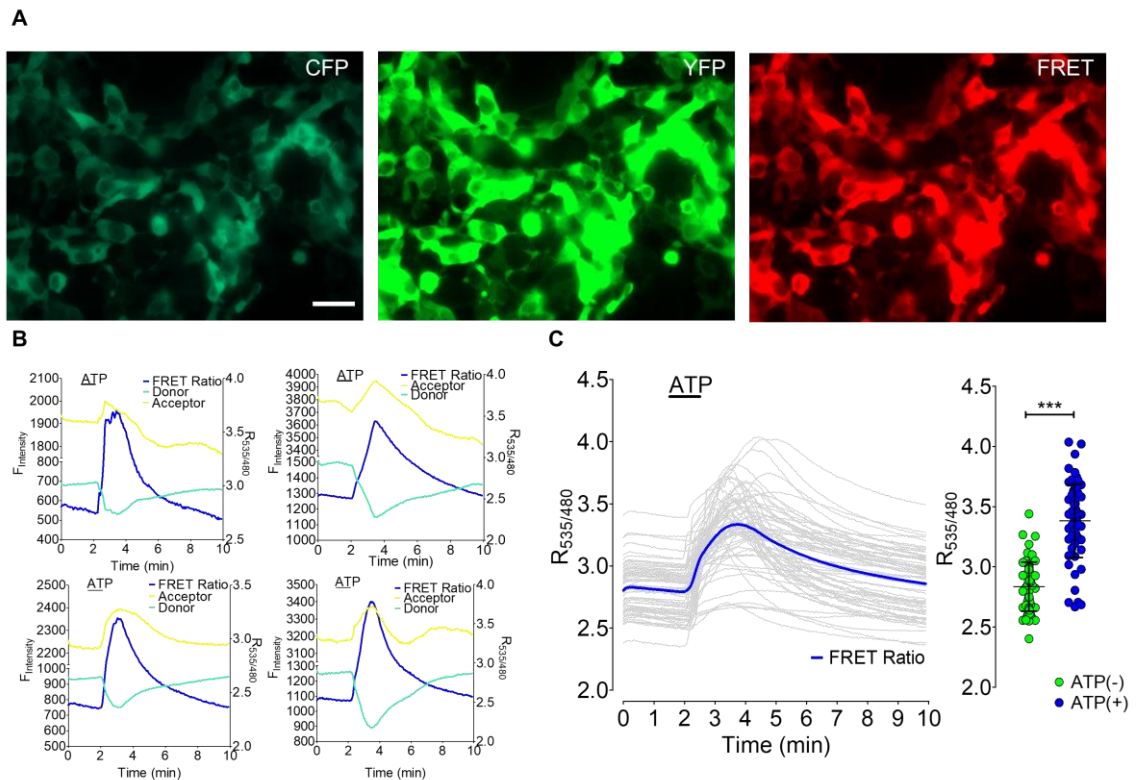


Figure 5.8: Live-cell FRET imaging using the D3-cpV calcium biosensor : (A) Representative fluorescence images of HEK293 cells expressing D3-cpV. Images are obtained proper filter according to channels (Excitation/Emission, CFP: 430/480, YFP: 515/535, FRET:430/535). The scale bar represents 20 μm . (B) The representative response of HEK293 cells expressing D3-cpV stimulated with 100 μM ATP as indicated. The cyan line represents the fluorescence intensity of Donor FP and the yellow line represents the fluorescence intensity of Acceptor FP. The blue line represents the FRET ratio. Left Y-axis represents the fluorescence intensity range and the right Y-axis represents the ratio range. (C) Left graphic shows the response of the cells expressing HEK293 cells expressing D3-cpV stimulated with 100 μM ATP as indicated. Grey lines represent single-cell responses and the blue line represents mean FRET ratio ($n=4/64$). The right scatter dot plot represents the maximum FRET ratio in the absence (green dots) or presence (blue dots) of the ATP ($n=4/64$). Data are shown in $\pm\text{SD}$ (Student's t-test, $p\text{-value} < 0.001$)

Notably, the significant overlap of the donor and acceptor signals (**Figure 5.9A**) which leads to so-called spectral bleed-through. In order to test spectral bleed-through, cells were transfected with two different constructs. One construct contains only mseCFP (CFP) as a fluorescent protein the other construct contains only cpVenus (YFP) as its fluorescent protein. Cells expressing these constructs individually were imaged under two different channels and total fluorescence intensity was measured (**Figure 5.9A**). As demonstrated in our experiments, this overlap does not significantly affect the performance of a FRET biosensor because of its wide dynamic range. In the case of FRET localization which is often used for interaction studies between proteins, the dynamic range can be limited, or the interaction can be spatially limited, hence, will lead

to the perish of the signals due to high signal-to-noise ratio. In order to overcome this limitation, different FRET calculation techniques have been developed in the recent past. One of these advanced FRET normalization techniques was developed by Youvan et al which allows quantitative FRET analysis (DC Youvan et al., 1997). Images obtained from the experiments above were used to calculate the FRET efficiency of the D3-cpV biosensor using ImageJ with an additional plug-in called FRET Colocalizer. **Figure 5.9B** shows pseudo colored FRET images in the presence or absence of the ATP.

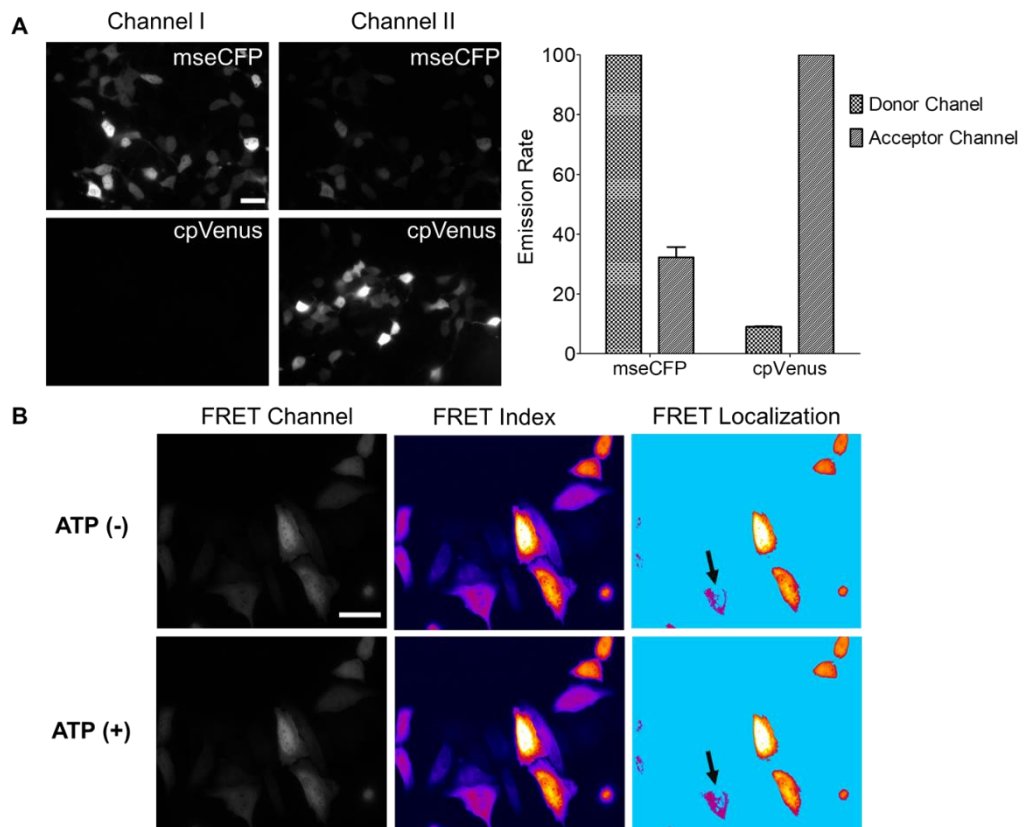


Figure 5.9: Spectral bleed through and localization FRET occurrence: (A) Representative monochromatic images shows the HEK293 cells expressing indicated fluorescent proteins only. Donor channel represent traditional filter sets for CFP (430/480) and acceptor channel represents traditional filter sets for YFP (515/535). Next box plot shows the normalized emission rate of fluorescent proteins in different channels (n=10) **(B)** Representative images of HeLa cells expressing D3-cpV stimulated with 100 μ M ATP. Left column shows the monochromatic images obtained using FRET channel in the absence (Upper panel) and the presence (Lower Panel) of ATP. Middle column represents FRET index of the cells in the absence (Upper panel) and the presence (Lower Panel) of ATP. High FRET areas represented with white color and low FRET areas indicated with dark blue colors. Right panel shows the localization of FRET occurrence in the cells. Black arrow shows representative FRET changes in the absence (Upper panel) and the presence (Lower Panel) of ATP. Scale bar represents 20 μ m

5.2 Design and development of a novel Acetyl-CoA biosensor

To develop an Acetyl-CoA (AcCoA) biosensor, there should be a sensing domain which is specific to AcCoA. As a sensing domain for the sensors two proteins are used which can bind AcCoA. These proteins are aspartate 1-decarboxylase (PanD) and PanD regulatory factors (PanZ) which are the components of the pantothenate biosynthesis pathway (Monteiro et al., 2015). PanD and PanZ create an octameric structure upon binding of AcCoA and has an affinity around 100 nM in 1:1 stoichiometry (Monteiro et al., 2012). According to the binding kinetics of PanD and PanZ makes these proteins are good candidates for the sensing domain of novel AcCoA biosensor. To track, measure AcCoA in living cells we decided to design a FRET-based AcCoA sensor

5.2.1 A FRET-based Acetyl CoA Sensor

In order to design FRET-based Acetyl-CoA biosensor, fluorescent proteins (FPs) are selected as the most commonly used FRET pair mseCFP and cpVenus FPs are chosen. The basis of creating FRET-based sensors is to quantify molecules that cause FRET upon binding. Using this approach PanD was combined with mseCFP from N-terminus and PanZ was combined with cpVenus from its C-terminus and these constructs are inserted in CMV driven mammalian expression vectors. The construct-design of these two genetically encoded fluorescent biosensors are depicted in **Figure 5.12A**. Molecular models of the AcCoA biosensors are shown in **Figure 5.12B**. Under AcCoA free condition these sensors are found in separated from each other. In the case of AcCoA binding, these two biosensors come up in proximity with a distance around 87 Å (**Figure 5.12B** lower panel). Proximity is important in the case of FRET sensors because energy transfer should occur within a Förster Radius which has a cut-off in 100 Å (Sekar & Periasamy, 2003).

To localize these sensors to mitochondria, COX8 tandems are integrated to the N-termini of each sensor. The reason for creating mitochondria-targeted genetically encoded fluorescent biosensors to discover AcCoA metabolism in mitochondria. AcCoA enters

mitochondria as an initiator of the KREBS cycle in oxidative phosphorylation and, it's the turn-on switch for this kind of energy metabolism in eukaryotic cells.

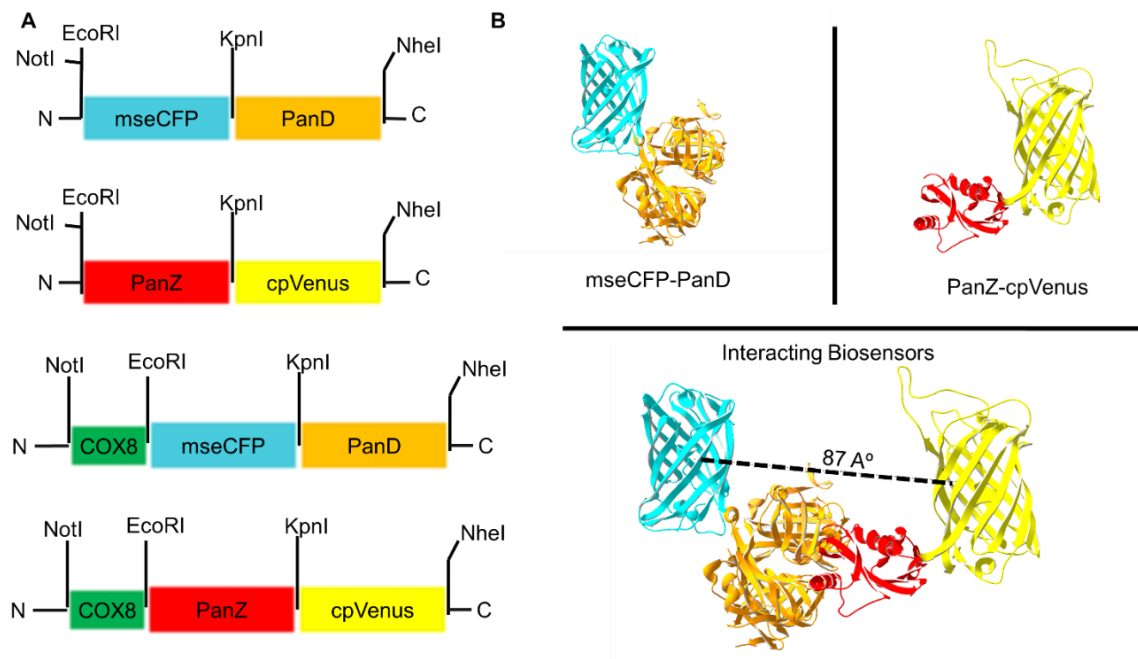


Figure 5.10: Design of a novel FRET-based Acetyl CoA sensor : (A) Schematic representation of construct design: mseCFP-PanD, PanZ-cpVenus, mito-mseCFP-PanD, mito-PanZ-cpVenus from top to bottom. (B) Molecular models of AcCoA biosensors: mseCFP-PanD (Right Panel), PanZ-cpVenus (Left Panel), Interaction of these two sensors with an 87 Å distance

In order to test whether FPs assembled and their localization correctly, plasmids transfected to HEK293 and HeLa cells. In **Figure 5.13** untargeted and mitochondria-targeted genetically encoded fluorescent biosensors are shown. N terminal COX8 tandem addition leads to localization of genetically encoded biosensor to mitochondria only.

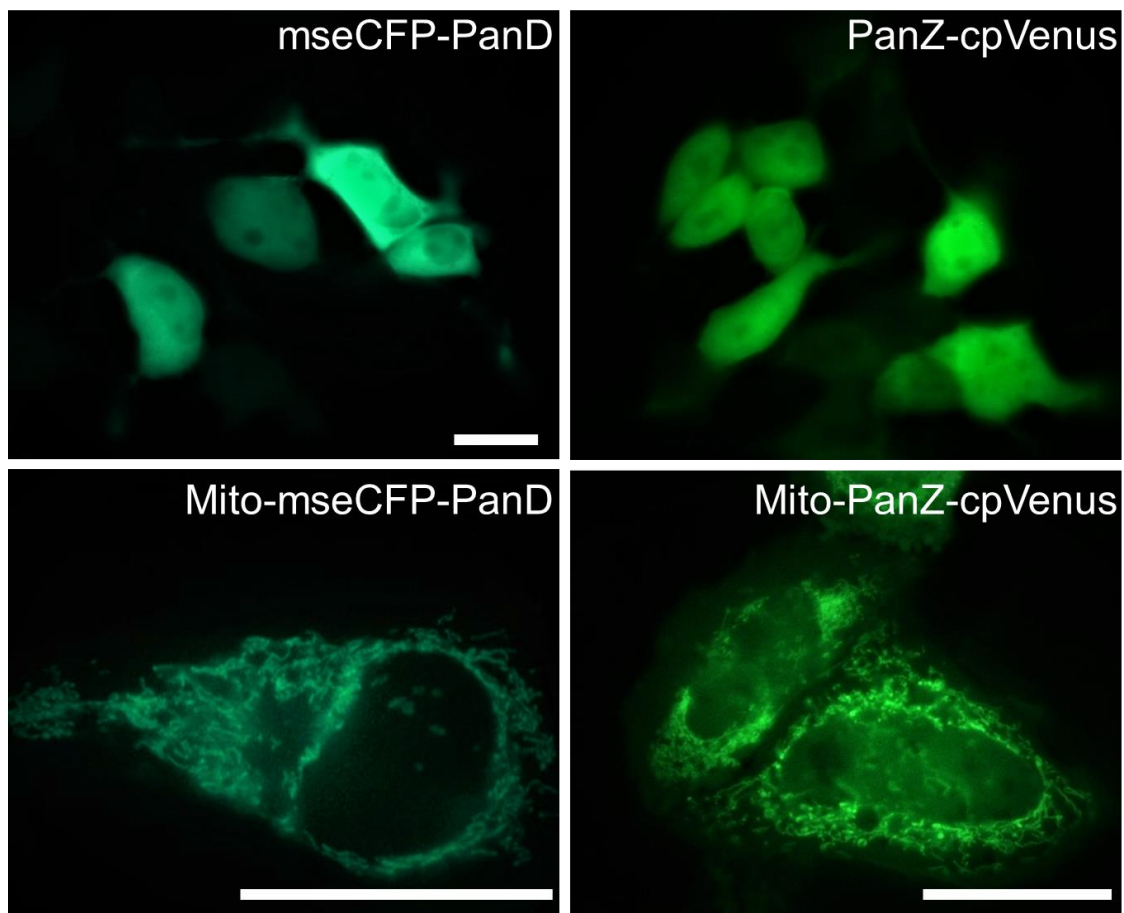


Figure 5.11: Visualization of novel Acetyl CoA Sensor: Fluorescence images of AcCoA sensors. HEK293 (Upper Panel) transfected with AcCoA biosensors individually mseCFP-PanD and PanZ-cpVenus respectively. HeLa cells (Lower panel) transfected with mitochondria-targeted AcCoA biosensors individually mito-mseCFP-PanD and mito-PanZ-cpVenus and visualized using 400X magnification. Scale bars represent 20 μm .

6 Discussion

Genetically encoded fluorescent biosensors are powerful tools to discover what is happening inside a cell. However, high-resolution fluorescence microscopy can be expensive because of the requirement of special filter sets, light sources, special objectives, and cameras due to the complex optical mechanisms that are being exploited in biosensors. Around half of the existing biosensors are FRET-based, which require sophisticated optical devices and the capability of dual recording for real-time imaging. Luckily, in the past few years, many biosensors were re-engineered to single FP-based probes that permit imaging using only one single wavelength. In this study, I aimed to show that many single FP based genetically encoded sensors can be used without special devices. At the beginning of my thesis, I had only a simple epifluorescence microscope available equipped with three standard filter cubes (blue, green, red) and a simple LED light source to excite at the wavelengths 360nm, 480nm, and 555nm, respectively, and a 20x air objective. Notably, the filters were to operate manually. This affordable and small microscope proved to be suitable when I tested various genetically encoded fluorescent biosensors including the most sophisticated and single-FP based biosensor.

First, I tested the geNOps, which are single FP bases biosensors for live-cell imaging of NO in single cells. geNOps are available in five different colors ranging from cyan to orange. Due to the lack of proper filters, I could only test the green variant and the orange variant on our microscope. My first attempt was to investigate whether the exposure time of the NO liberating chemical NOC-7 affects the response quality of geNOps. As shown in figure 5.1, the sensitivity and imaging quality of our imaging system proved to be very good as I could even resolve the differences in the NO profile between 15 and 30 seconds exposure to NOC-7. Moreover, longer exposure of NOC-7 yielded an increased amplitude of the geNOps signal while the on the kinetics of geNOps remained unaffected under, demonstrating the high responsiveness of the probe, and the capability of the imaging system to temporally resolve differences in such short NO donor treatment.

Unexpectedly, I also found that the orange variant of geNOps yielded a 12% maximum amplitude in response to NOC-7, which is equal to the green variant of geNOps. However, in the original article, the authors showed that the green variant amplitude is 50% higher compared to the orange geNOps. This observation and discordance in the biosensors' behavior demonstrate, that each biosensor needs to be tested and carefully characterized if a new imaging system is intended to use. After this characterization step, I next attempted whether I can measure intracellular NO derived by eNOS for which I used HEK293 cells co-expressing the G-geNOp and RFP-based eNOS variants. As shown in figure 5.1, I first observed an unexpected phenomenon, namely the different expression patterns of co-transfected cells. Despite a very high transfection efficiency, I had to select cells only which were sufficiently co-expressing both constructs, geNOps, and the eNOS. In future studies, either stable cell lines can be generated or bicistronic constructs to avoid such different expression profiles. Nevertheless, my approach turned out to be suitable to measure endogenously produced NO by differentially targeted eNOS. Here I tested the WT and myristoylation deficient eNOS pharmacologically activated by the IP3 generating agonist ATP. In line with my expectations, the WT showed a slow and sluggish NO profile upon activation. However, in contrast to the literature, the myristoylation deficient eNOS showed myristoylation deficiency does not affect NO biosynthesis. In the literature, it was shown that myristoylation deficiency significantly affects the activity of eNOS and NO production (Sakoda et al., 1995). However, the authors used indirect NO measurement techniques called the Griess Assay which detects nitrate which is a product of NO. Here we directly measured NO using the geNOps biosensors and showed that there is no significant difference in NO production of eNOS whether anchored to the caveolae or soluble in the cytosol (Figure 5.4). These findings demonstrate that a simple one channel epifluorescence microscope can be used to study the complex biochemistry of NO on the level of single cells.

I next tried to test the latest version HyPer7 version of the well-established H₂O₂ biosensors, which was published in March 2020, namely during my master's studies. Notably, there are two variants of HyPer7, a ratiometric HyPer7.2, and an intensimetric HyPer7.1. Due to the lack of an automatic filter turret, I tested the GFP based intensimetric and nuclear-targeted Hyper7.1-NLS. Indeed, the data I obtained using this novel biosensor in response to exogenous H₂O₂ unveiled that these probes are ultrasensitive and quickly reach the saturation phase. Until the third generation of HyPer (HyPer1-2-3), former experiments showed that the lower limit of extracellular H₂O₂, which activates HyPer in a living cell, is about 5 μM (Bilan & Belousov, 2016). This is in line with my experiments as I could not observe any response even with the ultrasensitive

HyPer7.1-NLS for extracellular H₂O₂ that was below 4 μM (Figure 5.5). However, my experiments also show that the novel HyPer7 instantly oxidizes and reaches the plateau very fast, which makes it suitable for the detection of even small amounts of intracellular H₂O₂, however, with the disadvantage that the probe immediately saturates. Nevertheless, in this set of experiments, I demonstrated that the novel HyPer7 can be utilized on our imaging systems using a standard GFP filter cube and no further equipment.

For Ca²⁺ imaging FRET-based probes are preferred because of their capability of quantification of Ca²⁺. However, due to the lack of a beam splitter or a second camera on our imaging system, I next investigated intracellular Ca²⁺ signals using intensimetric biosensors termed as GECOs. I used two variants of the red-shifted R-GECO1, one which is untargeted and another one that is mitochondria-targeted. To test whether I can utilize these probes on our imaging system, I tested MEF cells as a model system. Administration of the IP3 generating agonist ATP yielded a lower amplitude of mitochondrial Ca²⁺ signals compared to the cytosolic Ca²⁺ signals. Also, cytosolic the Ca²⁺ signal recovered significantly faster compared to the mitochondrial Ca²⁺ signal in these cell types. Furthermore, Ca²⁺ released to cytosol was slower compared to Ca²⁺ entering into the mitochondria. The situation was different in MGC cells, which have different properties compared to MEF cells. In these cells, due to their nature as neuronal glia cells, they have a higher potential to exchange ions because. In MGC, the amplitude of cytosolic Ca²⁺ signals was higher compared to mitochondrial Ca²⁺ signals. Also, the release of Ca²⁺ was significantly faster in cytosol compared to mitochondria. This is also valid for the recovery state of Ca²⁺. However, as mentioned before, GECOs are intensimetric biosensors and do not permit quantification, meaning that the amplitude of the GECO signal does not represent the quantity of Ca²⁺ that is released. Intensimetric GECOs only permit profiling of the signals. Using these powerful tools, I could clearly show that these probes are suitable for the investigation of Ca²⁺ signaling in the different compartments of the cell and, in different cell lines using our simple imaging device with only one RFP filter cube. I tried to distinguish Ca²⁺ profiles of the cytosol and mitochondria using R-GECO. As depicted in the results mitochondria has low elevations of Ca²⁺ but faster elevation rate. Finally, to try the last available filter cube on our system, which was the BFP filter cube that is predominantly used for DAPI staining, I attempted whether I can image the blue version of GECOs on our imaging system. As expected, I could trace Ca²⁺ signals in HeLa cells using B-GECO, however, the R-GECO signals appeared to show significantly higher amplitudes upon stimulation with ATP yet with lower variability. These tests demonstrate that there is a significant

difference in the Ca^{2+} detection profiles between the red and blue versions of GECOs demonstrating that these probes are only suitable for Ca^{2+} profiling but not quantification.

In the meantime, towards the last third of my diploma thesis our new FRET imaging system arrived. Using this opportunity, I tested Ca^{2+} signals in HEK cells using the FRET-based calcium sensor termed as D3cpV. The main point in these experiments was to show, that Ca^{2+} signaling can be measured via FRET and I wanted to exploit where these signalings occur in the cell exploiting a FRET index analysis plug-in in ImageJ. For this purpose, I choose the Youvan correction method to identify FRET occurring locales in the cells and identified spectral bleed through. Spectral bleed through prevents the correct FRET ratio in the experiments because we showed that donor fluorescent protein can be bleed through in the acceptor channel around 30%. Without calculating spectral bleed-through, results of the FRET experiments are not trustworthy. Also, I showed that even if the saturated pixels were obtained after the experiment, I could successfully localize FRET occurrence within cells.

Each of the findings in this study helped us to understand better how we can exploit these powerful tools using a simple fluorescence microscope. Here I showed two important things; (i) which parameters affect the performance of genetically encoded fluorescent biosensors and (ii) how we can use these biosensors to explain certain cell signaling in events. Without knowing how the biosensors are working or the parameters affecting their performance, we are not able to understand their read-outs. Moreover, I also showed how the choice of FP in genetically encoded biosensor affects the results of an experiment. Two different situations were shown here; the first one changing the colors of the FPs that are distant in the visible light spectrum. TagBFP belongs to B-GECO, and TagRFP belongs to R-GECO and showed significantly different responses. The other one is the changing colors of FPs that are in proximity in the visible light spectrum. EGFP belongs to G-geNOP, mKO.k, belongs to O-geNOP, and showed similar responses. The outcome of these experiments showed that multi-spectral experiments should be carefully designed because the specificity of each variant of the genetically encoded fluorescent biosensors is not the same. It is important to know these parameters before starting an experiment.

7 Conclusion

In this study, I have characterized and showed that a variety of intensimetric-based GEFB can be successfully employed on a simple LED-based epifluorescence microscope for live-cell imaging with high spatial and temporal resolution. Moreover, I have designed and generated a putative novel FRET-based GEFB for Acetyl-CoA that is either soluble in the cytosol or targeted to the mitochondria. In my doctorate studies, I will conduct specific tests and validation studies to further characterize this novel biosensor for its suitability for the quantification of Acetyl-CoA in live cells.

8 Bibliography

- Amaral, G., Bushee, J., Cordani, U. G., KAWASHITA, K., Reynolds, J. H., ALMEIDA, F. F. M. D. E., de Almeida, F. F. M., Hasui, Y., de Brito Neves, B. B., Fuck, R. A., Oldenzaal, Z., Guida, A., Tchalenko, J. S., Peacock, D. C. P., Sanderson, D. J., Rotevatn, A., Nixon, C. W., Rotevatn, A., Sanderson, D. J., ... Junho, M. do C. B. (2013). FRET and Colocalization Analyzer - User's Guide. *Journal of Petrology*, 369(1), 1689–1699. <https://doi.org/10.1017/CBO9781107415324.004>
- Andresen, M., Wahl, M. C., Stiel, A. C., Gräter, F., Schäfer, L. v., Trowitzsch, S., Weber, G., Eggeling, C., Grubmüller, H., Hell, S. W., & Jakobs, S. (2005). Structure and mechanism of the reversible photoswitch of a fluorescent protein. *Proceedings of the National Academy of Sciences of the United States of America*, 102(37), 13070–13074. <https://doi.org/10.1073/pnas.0502772102>
- Baehler, P. J., Biondi, R. M., van Bemmelen, M., Véron, M., & Reymond, C. D. (2002). Random insertion of green fluorescent protein into the regulatory subunit of cyclic adenosine monophosphate-dependent protein kinase. *Methods in Molecular Biology (Clifton, N.J.)*, 183(6), 57–68. <https://doi.org/10.1385/1-59259-280-5:057>
- Baird, G. S., Zacharias, D. A., & Tsien, R. Y. (1999). Circular permutation and receptor insertion within green fluorescent proteins. *Proceedings of the National Academy of Sciences of the United States of America*, 96(20), 11241–11246. <https://doi.org/10.1073/pnas.96.20.11241>
- Bajar, B. T., Wang, E. S., Zhang, S., Lin, M. Z., & Chu, J. (2016). A guide to fluorescent protein FRET pairs. *Sensors (Switzerland)*, 16(9), 1–24. <https://doi.org/10.3390/s16091488>
- Belousov, V. v., Fradkov, A. F., Lukyanov, K. A., Staroverov, D. B., Shakhbazov, K. S., Terskikh, A. v., & Lukyanov, S. (2006). Genetically encoded fluorescent indicator for intracellular hydrogen peroxide. *Nature Methods*, 3(4), 281–286. <https://doi.org/10.1038/nmeth866>
- Bilan, D. S., & Belousov, V. v. (2016). HyPer Family Probes: State of the Art. *Antioxidants and Redox Signaling*, 24(13), 731–751. <https://doi.org/10.1089/ars.2015.6586>

- Bokman, S. H., & Ward, W. W. (1981). Renaturation of Aequorea green-fluorescent protein. *Biochemical and Biophysical Research Communications*, 101(4), 1372–1380. [https://doi.org/10.1016/0006-291X\(81\)91599-0](https://doi.org/10.1016/0006-291X(81)91599-0)
- Brejč, K., Sixma, T. K., Kitts, P. A., Kain, S. R., Tsien, R. Y., Ormö, M., & Remington, S. J. (1997a). Structural basis for dual excitation and photoisomerization of the Aequorea victoria green fluorescent protein. *Proceedings of the National Academy of Sciences of the United States of America*, 94(6), 2306–2311. <https://doi.org/10.1073/pnas.94.6.2306>
- Brejč, K., Sixma, T. K., Kitts, P. A., Kain, S. R., Tsien, R. Y., Ormö, M., & Remington, S. J. (1997b). Structural basis for dual excitation and photoisomerization of the Aequorea victoria green fluorescent protein. *Proceedings of the National Academy of Sciences of the United States of America*, 94(6), 2306–2311. <https://doi.org/10.1073/pnas.94.6.2306>
- Chalfe, M., Inouye, S., Tsuji Frederick, I., Tu, Y., Euskirchen, G., Ward William, W., & Prasher Douglas, C. (1994). Expression of the gene and fluorescence characteristics of the recombinant protein Green fluorescent protein as a marker for gene expression. *Fed. Eur. Biochem. Letters*, 341(5148), 277–280.
- Chattoraj, M., King, B. A., Bublitz, G. U., & Boxer, S. G. (1996). Ultra-fast excited state dynamics in green fluorescent protein: Multiple states and proton transfer. *Proceedings of the National Academy of Sciences of the United States of America*, 93(16), 8362–8367. <https://doi.org/10.1073/pnas.93.16.8362>
- Chudakov, D. M., Feofanov, A. v., Mudrik, N. N., Lukyanov, S., & Lukyanov, K. A. (2003). Chromophore environment provides clue to “kindling fluorescent protein” riddle. *Journal of Biological Chemistry*, 278(9), 7215–7219. <https://doi.org/10.1074/jbc.M211988200>
- Chudakov, D. M., Matz, M. v., Lukyanov, S., & Lukyanov, K. A. (2010). Fluorescent proteins and their applications in imaging living cells and tissues. *Physiological Reviews*, 90(3), 1103–1163. <https://doi.org/10.1152/physrev.00038.2009>
- Coling, D., & Kachar, B. (1998). Principles and Application of Fluorescence Microscopy. *Current Protocols in Molecular Biology*, 44(1), 1–11. <https://doi.org/10.1002/0471142727.mb1410s44>

- Combs, C. A. (2010). Fluorescence microscopy: A concise guide to current imaging methods. *Current Protocols in Neuroscience*, SUPPL.50, 1–19. <https://doi.org/10.1002/0471142301.ns0205s00>
- Corish, P., & Tyler-Smith, C. (1999). Attenuation of green fluorescent protein half-life in mammalian cells. *Protein Engineering*, 12(12), 1035–1040. <https://doi.org/10.1093/protein/12.12.1035>
- Cubitt, A. B., Heim, R., Adams, S. R., Boyd, A. E., Gross, L. A., & Tsien, R. Y. (1995). Understanding, improving and using green fluorescent proteins. *Trends in Biochemical Sciences*, 20(11), 448–455. [https://doi.org/10.1016/S0968-0004\(00\)89099-4](https://doi.org/10.1016/S0968-0004(00)89099-4)
- Davidson W. Michael. (2003). *Molecular Expressions Microscopy Primer: Anatomy of the Microscope - Microscope Light Sources*. Molecular Expressions. <https://micro.magnet.fsu.edu/primer/anatomy/lightsource/home.html>
- DC Youvan, CM Silva, EJ Bylina, WJ Coleman, MR Dilworth, & MM Yang. (1997). Calibration of Fluorescence Resonance Energy Transfer in Microscopy Using Genetically Engineered GFP Derivatives on Nickel Chelating Beads. *Biotechnology et Alia*, 3(January), 1–18. <https://doi.org/http://www.et-al.com/searchable/abstracts/abstract3.html>
- Eroglu, E., Gottschalk, B., Charoensin, S., Blass, S., Bischof, H., Rost, R., Madreiter-Sokolowski, C. T., Pelzmann, B., Bernhart, E., Sattler, W., Hallstrom, S., Malinski, T., Waldeck-Weiermair, M., Graier, W. F., & Malli, R. (2016). Development of novel FP-based probes for live-cell imaging of nitric oxide dynamics. *Nature Communications*, 7. <https://doi.org/10.1038/ncomms10623>
- Frommer, W. B., Davidson, M. W., & Campbell, R. E. (2009). Genetically encoded biosensors based on engineered fluorescent proteins. *Chemical Society Reviews*, 38(10), 2833–2841. <https://doi.org/10.1039/b907749a>
- Gallegos, L. L., Kunkel, M. T., & Newton, A. C. (2006). Targeting protein kinase C activity reporter to discrete intracellular regions reveals spatiotemporal differences in agonist-dependent signaling. *Journal of Biological Chemistry*, 281(41), 30947–30956. <https://doi.org/10.1074/jbc.M603741200>
- Gleeson, P. A., Teasdale, R. D., & Burke, J. (1994). Targeting of proteins to the Golgi apparatus. *Glycoconjugate Journal*, 11(5), 381–394. <https://doi.org/10.1007/BF00731273>

- Gould, S. J., Keller, G. A., Hosken, N., Wilkinson, J., & Subramani, S. (1989). A conserved tripeptide sorts proteins to peroxisomes. *Journal of Cell Biology*, *108*(5), 1657–1664. <https://doi.org/10.1083/jcb.108.5.1657>
- Greenwald, E. C., Mehta, S., & Zhang, J. (2018). Genetically encoded fluorescent biosensors illuminate the spatiotemporal regulation of signaling networks. *Chemical Reviews*, *118*(24), 11707–11794. <https://doi.org/10.1021/acs.chemrev.8b00333>
- Griesbeck, O. (2004). Fluorescent proteins as sensors for cellular functions. *Current Opinion in Neurobiology*, *14*(5), 636–641. <https://doi.org/10.1016/j.conb.2004.08.002>
- Heim, R., & Tsien, R. Y. (1996). Engineering green fluorescent protein for improved brightness, longer wavelengths and fluorescence resonance energy transfer. *Current Biology*, *6*(2), 178–182. [https://doi.org/10.1016/S0960-9822\(02\)00450-5](https://doi.org/10.1016/S0960-9822(02)00450-5)
- Hell, S. W. (2003). Toward fluorescence nanoscopy. *Nature Biotechnology*, *21*(11), 1347–1355. <https://doi.org/10.1038/nbt895>
- Jayaraman, S., Haggie, P., Wachter, R. M., Remington, S. J., & Verkman, A. S. (2000). Mechanism and cellular applications of a green fluorescent protein-based halide sensor. *Journal of Biological Chemistry*, *275*(9), 6047–6050. <https://doi.org/10.1074/jbc.275.9.6047>
- Johansson, K., Cebula, M., Rengby, O., Dreij, K., Carlström, K. E., Sigmundsson, K., Piehl, F., & Arnér, E. S. J. (2017). Cross Talk in HEK293 Cells between Nrf2, HIF, and NF-κB Activities upon Challenges with Redox Therapeutics Characterized with Single-Cell Resolution. *Antioxidants and Redox Signaling*, *26*(6), 229–246. <https://doi.org/10.1089/ars.2015.6419>
- Kalko, E. K. v, Dukas, R., Ratcliffe, J. M., Teeling, E. C., Haven, N., Fattu, J. M., Bates, M. E., Simmons, J. a, Riquimaroux, H., Surlykke, a, Bouffard, F. H., Lee, D. N., Dear, S. P., Horiuchi, T. K., Krishnaprasad, P. S., Moss, C. F., Schuller, G., Brudzynski, S. M., Syme, D. a, ... Vater, M. a. (2011). An Expanded Palette of Genetically. *Cell*, *557*(September), 1888–1891. <https://doi.org/10.1126/science.1208592>
- Keller, H. E. (2006). Objective Lenses for Confocal Microscopy. In J. B. Pawley (Ed.), *Handbook Of Biological Confocal Microscopy* (pp. 145–161). Springer US. https://doi.org/10.1007/978-0-387-45524-2_7

- Kneen, M., Farinas, J., Li, Y., & Verkman, A. S. (1998). Green fluorescent protein as a noninvasive intracellular pH indicator. *Biophysical Journal*, *74*(3), 1591–1599. [https://doi.org/10.1016/S0006-3495\(98\)77870-1](https://doi.org/10.1016/S0006-3495(98)77870-1)
- Kogure, T., Karasawa, S., Araki, T., Saito, K., Kinjo, M., & Miyawaki, A. (2006). A fluorescent variant of a protein from the stony coral *Montipora* facilitates dual-color single-laser fluorescence cross-correlation spectroscopy. *Nature Biotechnology*, *24*(5), 577–581. <https://doi.org/10.1038/nbt1207>
- Lam, A. J., St-Pierre, F., Gong, Y., Marshall, J. D., Cranfill, P. J., Baird, M. A., McKeown, M. R., Wiedenmann, J., Davidson, M. W., Schnitzer, M. J., Tsien, R. Y., & Lin, M. Z. (2012). Improving FRET dynamic range with bright green and red fluorescent proteins. *Nature Methods*, *9*(10), 1005–1012. <https://doi.org/10.1038/nmeth.2171>
- Lemay, N. P., Morgan, A. L., Archer, E. J., Dickson, L. A., Megley, C. M., & Zimmer, M. (2008). The role of the tight-turn, broken hydrogen bonding, Glu222 and Arg96 in the post-translational green fluorescent protein chromophore formation. *Chemical Physics*, *348*(1–3), 152–160. <https://doi.org/10.1016/j.chemphys.2008.02.055>
- Luger, K., Hommel, U., Herold, M., Hofsteenge, J., & Kirschner, K. (1989). Correct folding of circularly permuted variants of a $\beta\alpha$ barrel enzyme in vivo. *Science*, *243*(4888), 206–210. <https://doi.org/10.1126/science.2643160>
- Masedunskas, A., Sramkova, M., Parente, L., & Weigert, R. (2013). Cell Imaging Techniques. In *Methods in Molecular Biology* (Vol. 931, Issue 1). <https://doi.org/10.1007/978-1-62703-056-4>
- Mats, O., Andrew, B. C., Karen, K., Larry, A. G., Tsien, R. Y., & Remington, S. J. (1996). Crystal structure of the *Aequorea victoria* green fluorescent protein. *Science*, *273*(5280), 1392–1395. <https://doi.org/10.1126/science.273.5280.1392>
- McAnaney, T. B., Park, E. S., Hanson, G. T., Remington, S. J., & Boxer, S. G. (2002). Green fluorescent protein variants as ratiometric dual emission pH sensors. 2. Excited-state dynamics. *Biochemistry*, *41*(52), 15489–15494. <https://doi.org/10.1021/bi026610o>
- Miyawaki, A. (2003). Visualization of the spatial and temporal dynamics of intracellular signaling. *Developmental Cell*, *4*(3), 295–305. [https://doi.org/10.1016/S1534-5807\(03\)00060-1](https://doi.org/10.1016/S1534-5807(03)00060-1)
- Monteiro, D. C. F., Patel, V., Bartlett, C. P., Nozaki, S., Grant, T. D., Gowdy, J. A., Thompson, G. S., Kalverda, A. P., Snell, E. H., Niki, H., Pearson, A. R., & Webb,

- M. E. (2015). The structure of the PanD/PanZ protein complex reveals negative feedback regulation of pantothenate biosynthesis by coenzyme a. *Chemistry and Biology*, 22(4), 492–503. <https://doi.org/10.1016/j.chembiol.2015.03.017>
- Monteiro, D. C. F., Rugen, M. D., Shepherd, D., Nozaki, S., Niki, H., & Webb, M. E. (2012). Formation of a heterooctameric complex between aspartate α -decarboxylase and its cognate activating factor, PanZ, is CoA-dependent. *Biochemical and Biophysical Research Communications*, 426(3), 350–355. <https://doi.org/10.1016/j.bbrc.2012.08.084>
- Moradpour, D., Evans, M. J., Gosert, R., Yuan, Z., Blum, H. E., Goff, S. P., Lindenbach, B. D., & Rice, C. M. (2004). Insertion of Green Fluorescent Protein into Nonstructural Protein 5A Allows Direct Visualization of Functional Hepatitis C Virus Replication Complexes. *Journal of Virology*, 78(14), 7400–7409. <https://doi.org/10.1128/jvi.78.14.7400-7409.2004>
- Moser, C., Mayr, T., & Klimant, I. (2006). Filter cubes with built-in ultrabright light-emitting diodes as exchangeable excitation light sources in fluorescence. *Journal of Microscopy*, 222(January), 135–140. <https://doi.org/10.1111/j.1365-2818.2006.01581.x>
- Nguyen, A. W., & Daugherty, P. S. (2005). Evolutionary optimization of fluorescent proteins for intracellular FRET. *Nature Biotechnology*, 23(3), 355–360. <https://doi.org/10.1038/nbt1066>
- Palmer, A. E., Giacomello, M., Kortemme, T., Hires, S. A., Lev-Ram, V., Baker, D., & Tsien, R. Y. (2006). Ca²⁺ Indicators Based on Computationally Redesigned Calmodulin-Peptide Pairs. *Chemistry and Biology*, 13(5), 521–530. <https://doi.org/10.1016/j.chembiol.2006.03.007>
- Palmer, A. E., Jin, C., Reed, J. C., & Tsien, R. Y. (2004). Bcl-2-mediated alterations in endoplasmic reticulum Ca²⁺ analyzed with an improved genetically encoded fluorescent sensor. *Proceedings of the National Academy of Sciences of the United States of America*, 101(50), 17404–17409. <https://doi.org/10.1073/pnas.0408030101>
- Piston, D. W., & Kremers, G. J. (2007). Fluorescent protein FRET: the good, the bad and the ugly. *Trends in Biochemical Sciences*, 32(9), 407–414. <https://doi.org/10.1016/j.tibs.2007.08.003>

- Prasher, D. C., Eckenrode, V. K., Ward, W. W., Prendergast, F. G., & Cormier, M. J. (1992). Primary structure of the *Aequorea victoria* green-fluorescent protein. *Gene*, *111*(2), 229–233. [https://doi.org/10.1016/0378-1119\(92\)90691-H](https://doi.org/10.1016/0378-1119(92)90691-H)
- Renz, M. (2013). Fluorescence microscopy-A historical and technical perspective. *Cytometry Part A*, *83*(9), 767–779. <https://doi.org/10.1002/cyto.a.22295>
- Rodriguez, E. A., Campbell, R. E., Lin, J. Y., Lin, M. Z., Miyawaki, A., Palmer, A. E., Shu, X., Zhang, J., & Tsien, R. Y. (2017). The Growing and Glowing Toolbox of Fluorescent and Photoactive Proteins. *Trends in Biochemical Sciences*, *42*(2), 111–129. <https://doi.org/10.1016/j.tibs.2016.09.010>
- Sakaue-Sawano, A., Kurokawa, H., Morimura, T., Hanyu, A., Hama, H., Osawa, H., Kashiwagi, S., Fukami, K., Miyata, T., Miyoshi, H., Imamura, T., Ogawa, M., Masai, H., & Miyawaki, A. (2008). Visualizing Spatiotemporal Dynamics of Multicellular Cell-Cycle Progression. *Cell*, *132*(3), 487–498. <https://doi.org/10.1016/j.cell.2007.12.033>
- Sakoda, T., Hirata, K. ichi, Kuroda, R., Miki, N., Suematsu, M., Kawashima, S., & Yokoyama, M. (1995). Myristoylation of endothelial cell nitric oxide synthase is important for extracellular release of nitric oxide. *Molecular and Cellular Biochemistry*, *152*(2), 143–148. <https://doi.org/10.1007/BF01076076>
- Scott, B. L., & Hoppe, A. D. (2015). Optimizing fluorescent protein trios for 3-Way FRET imaging of protein interactions in living cells. *Scientific Reports*, *5*, 1–13. <https://doi.org/10.1038/srep10270>
- Sekar, R. B., & Periasamy, A. (2003). Fluorescence resonance energy transfer (FRET) microscopy imaging of live cell protein localizations. *Journal of Cell Biology*, *160*(5), 629–633. <https://doi.org/10.1083/jcb.200210140>
- Shaner, N. C., Patterson, G. H., & Davidson, M. W. (2007). Advances in fluorescent protein technology. *Journal of Cell Science*, *120*(24), 4247–4260. <https://doi.org/10.1242/jcs.005801>
- Shimoura, O., Johnson, F. H., & Saiga, Y. (1962). Extraction, purification and properties of aequorin, a bioluminescent. *Journal of Cellular and Comparative Physiology*, *59*(165), 223–239. <https://doi.org/10.1002/jcp.1030590302>
- Spring, K. R. (2007). Cameras for Digital Microscopy. *Methods in Cell Biology*, *81*(06), 171–186. [https://doi.org/10.1016/S0091-679X\(06\)81010-1](https://doi.org/10.1016/S0091-679X(06)81010-1)

- Starr, D. A. (2011). Fluorescence Microscopy. *Physiology & Behavior*, 176(1), 139–148. <https://doi.org/10.1016/j.physbeh.2017.03.040>
- Stokes, G. (1852). On the change of refractibility of light. *Philos Trans R Soc London*, 142, 463–562.
- St-Pierre, F., Marshall, J. D., Yang, Y., Gong, Y., Schnitzer, M. J., & Lin, M. Z. (2014). High-fidelity optical reporting of neuronal electrical activity with an ultrafast fluorescent voltage sensor. *Nature Neuroscience*, 17(6), 884–889. <https://doi.org/10.1038/nn.3709>
- Subach, F. v., Subach, O. M., Gundorov, I. S., Morozova, K. S., Piatkevich, K. D., Cuervo, A. M., & Verkhusha, V. v. (2009). Monomeric fluorescent timers that change color from blue to red report on cellular trafficking. *Nature Chemical Biology*, 5(2), 118–126. <https://doi.org/10.1038/nchembio.138>
- Tsien, R. Y. (1998). the Green Fluorescent Protein. *Annual Review of Biochemistry*, 67(1), 509–544. <https://doi.org/10.1146/annurev.biochem.67.1.509>
- Wang, L., & Tsien, R. Y. (2006). Evolving proteins in mammalian cells using somatic hypermutation. *Nature Protocols*, 1(3), 1346–1350. <https://doi.org/10.1038/nprot.2006.243>
- Webb, D. J., Donais, K., Whitmore, L. A., Thomas, S. M., Turner, C. E., Parsons, J. T., & Horwitz, A. F. (2004). FAK-Src signalling through paxillin, ERK and MLCK regulates adhesion disassembly. *Nature Cell Biology*, 6(2), 154–161. <https://doi.org/10.1038/ncb1094>
- Wen, W., Meinkoth, J. L., Tsien, R. Y., & Taylor, S. S. (1995). Identification of a signal for rapid export of proteins from the nucleus. *Cell*, 82(3), 463–473. [https://doi.org/10.1016/0092-8674\(95\)90435-2](https://doi.org/10.1016/0092-8674(95)90435-2)
- Wriggers, W., Chakravarty, S., & Jennings, P. A. (2005). Control of protein functional dynamics by peptide linkers. *Biopolymers - Peptide Science Section*, 80(6), 736–746. <https://doi.org/10.1002/bip.20291>
- Yang, F. (1996). The molecular structure of green fluorescent protein. *Nat. Biotechnol.*, 14(October), 1246–1251. <https://doi.org/10.2210/pdb1gfl/pdb>
- Zarowny, L., Aggarwal, A., Rutten, V. M. S., Kolb, I., Project, T. G., Patel, R., Huang, H. Y., Chang, Y. F., Phan, T., Kanyo, R., Ahrens, M. B., Allison, W. T., Podgorski, K., & Campbell, R. E. (2020). A bright and high-performance genetically encoded Ca²⁺

indicator based on mNeonGreen fluorescent protein. *ACS Sensors*.
<https://doi.org/10.1021/acssensors.0c00279>